Theses and Dissertations

December 2012

Material Behavior Characterization of a Thin Film Polymer Used in Lithium-Ion Batteries

Michael James Martinsen
University of Wisconsin-Milwaukee

MATERIAL BEHAVIOR CHARACTERIZATION OF A THIN FILM POLYMER

USED IN LITHIUM-ION BATTERIES

by

Michael J Martinsen

A Thesis Submitted in

Partial Fulfillment of the

Requirements for the Degree of

Master of Science

in Engineering

at

The University of Wisconsin-Milwaukee

December 2012

ABSTRACT

MATERIALS TESTING OF A LITHIUM ION BATTERY SEPARATOR FOR
USE IN FINITE ELEMENT ANALYSIS

by

Michael J Martinsen

The University of Wisconsin-Milwaukee, 2012
Under the Supervision of Professor Ilya Avdeev

The use of lithium-ion batteries in the automotive industry
has become increasingly popular. As more hybrid and
electric vehicles take to the road an understanding of how
these batteries will behave structurally will be of greater
concern. Impact testing can give a valuable overview of
the strengths and weaknesses of a battery's design,
however, these tests can be time consuming, expensive, and
dangerous. Finite element analysis can deliver a reliable
low cost approximation of physical testing results. The
accuracy of FE results depends greatly on the mathematical
representation of the material properties of Li-ion battery
components. In this study, the material properties of thin
film polymer used as a separator between an anode and a
cathode of a lithium ion battery are tested experimentally
under various temperatures, strain rates, and solvent
saturations. Due to the anisotropy of the material, two

similar sets of experiments were conducted on the material in perpendicular directions. It was found that temperature and strain rate have a nearly linear effect on the stress experienced by the material. Additionally, saturating the separator material in a common lithium ion solvent resulted in its softening with a positive effect on its toughness. Two viscoplastic constitutive equations developed for modeling polymeric materials were employed to model the experimental data.

TABLE OF CONTENTS

LIST OF FIGURES

LIST OF TABLES

ACKNOWLEDGMENTS

INTRODUCTION

The main purpose of a lithium ion battery separator is to prevent contact between the anode and the cathode, while facilitating the diffusion of ions between the two electrodes (Gaines & Cuenca, 2000). Lithium ions are able to flow between the two electrodes via an electrolyte medium through small pores in the separator. The electrolyte is a lithium salt that has been dissolved in an organic solvent(Mikolajczak, Kahn, White, & Long, 2012). Typical separators are between 20 and 30 microns thick(Huang, 2010). Although the demand for thinner separators is present, they must be strong enough to withstand the forces that occur during the winding process that is seen in both the prismatic and cylindrical Li-ion battery design (Arora & Zhang, 2004).

Lithium ion battery separators are produced by a number of manufacturers and are generally made from a polyolefin, mainly polyethylene (PE), polypropylene (PP), or a combination of both. The manufacturing process of these thin film micro porous membranes can vary leading to large changes in material properties. The two main manufacturing

processes are commonly known as (1) wet- and (2) dry manufacturing (Huang, 2010). With the dry manufacturing process the olefin is extruded above its melting point in order to bring the separator to its designated thickness, and then annealed. Additional stretching of the separator induces small micro pores that are aligned in a linear fashion. Due to the organization of these micro pores the separator's mechanical properties are anisotropic and show the greatest strength in its direction of stretch (machine direction). For the "wet" process a polyolefin resin is mixed with a hydrocarbon then heated until the mixture melts. The melted mixture is then extruded as a sheet and the liquid is extracted with a volatile liquid leaving behind micro pores (Huang, 2010; Love, 2011). The mechanical properties of these microporus separators are generally more isotropic since the voids are not introduced mechanically(Love, 2011).

The general morphology of a polyolefin battery separator is that of a semi-crystalline, composed of a crystalline phase and an amorphous phase. Separator material properties have shown to be highly temperature dependent (Love, 2011). The elastic characteristics of the polymer can be attributed to the stretching of the amorphous region where entangled strands of polymer chains become aligned.

Plastic deformation is observed after the amorphous chains become ordered and begin to distribute load to the crystalline phase causing slippage or separation of the crystal planes to occur (Drozdov & deC. Christiansen, 2007).

Several constitutive models have been developed with varying degrees of accuracy to model the micro mechanics of semi crystalline polymers (Bergström, Kurtz, Rimnac, & Edidin, 2002; Chaboche, 2008; Nikolov & Doghri, 2000).

Saturation levels can have a significant effect on the mechanical properties of a battery separator. Research has shown that submerging a separator material in an electrolyte solvent can greatly decrease the modulus and strength of the material (Sheidaei, Xiao, Huang, & Hitt, 2011). Changing the type of electrolyte solvent can also influence how the separator will behave mechanically.

In this study, a battery separator composed of both polyethylene and polypropylene is tested under tension with varying temperatures, strain rates, and solvent saturations. An evaluation of the constitutive model's ability to capture the material's elastic, plastic, and strain hardening regions for various strain rates and temperatures was conducted.

MATERIALS

Commercially available Celgard C480 tri-layered separator material with a thickness of 22.5 microns was used in all tests (Table 1). The micro porous separator consists of a polyethylene layer sandwiched between two layers of polypropylene. The center polyethylene layer is added as a safety mechanism, designed to melt and block the flow of ions in case of thermal runaway. Pores are induced on the material through stretching which generates a distinct pore pattern (Figure 1).

Basic Film Properties	Unit of Measurement	Typical Value
Thickness	µm	21.5
Porosity	%	50%
PP Pore Size	µm	0.038
TD Shrinkage @90°C/1hr	%	0.00%
MD Shrinkage @90°C/1hr	%	<5.0%
Puncture Strength (g)	Grams	>400
TD Tensile Strength	kgf/cm^2	140
TD Tensile Strength	kgf/cm^2	2195

TABLE 1 PROPERTIES OF CELGARD C480 TRILAYERD SEPARATOR

(Celgard, 2012)
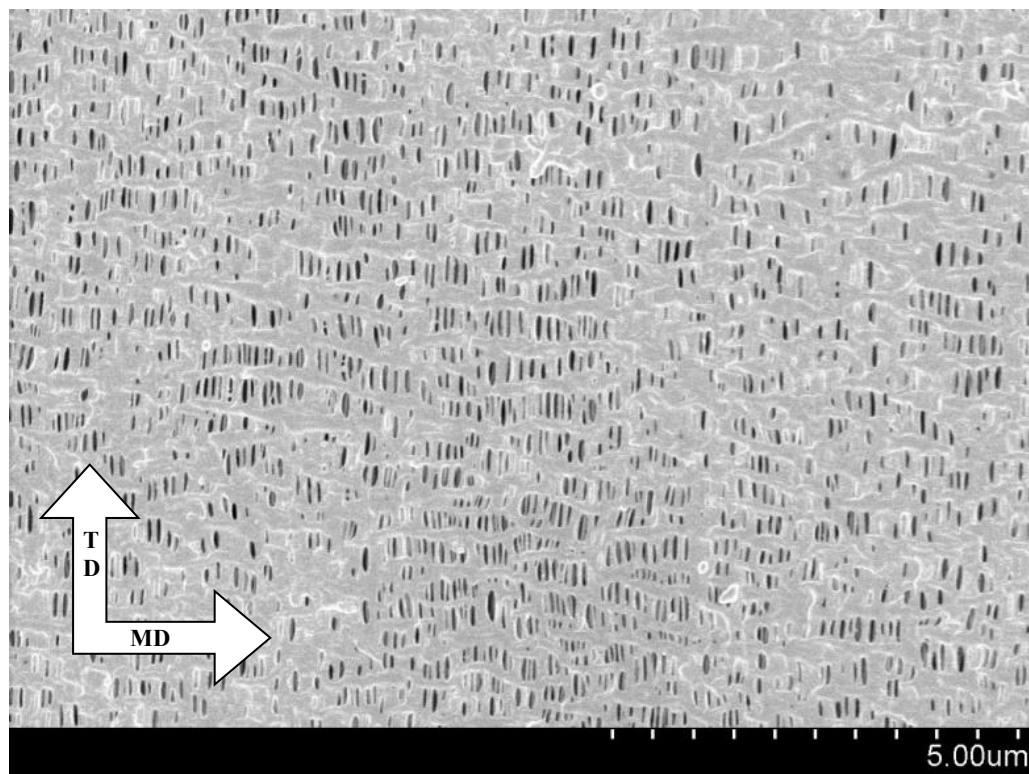
FIGURE 1 CELGARD SEPARATOR MATERIAL MAGNIFIED AT 10K

(TD=TRANSVERSE DIRECTION, MD=MACHINE DIRECTION).

The material exhibits highly anisotropic behavior and is significantly stronger in the machine direction compared to the transverse direction.

EXPERIMENTAL SETUP

Dry Conditions

Each 22.5 micron thick test sample was cut to 6 mm wide strips leading to a cross sectional area of 0.135 mm^2. To assure that the sample geometry remained constant a 1/8"

thick aluminum template was milled to be 6mm wide by 30mm long (Figure 2). All samples were cut with an X-acto® knife fitted with a #2 blade along the perimeter of the aluminum template.   The samples were loaded into a TA RSA III Dynamic Mechanical Analyzer (DMA) (*RSA III Rheometrics System Analyzer*, 2005) and given a gauge length of 15mm (Figure 3).   Each of the samples was clamped into the tensile fixture with a torque wrench to maintain exact clamping forces through all the tests.
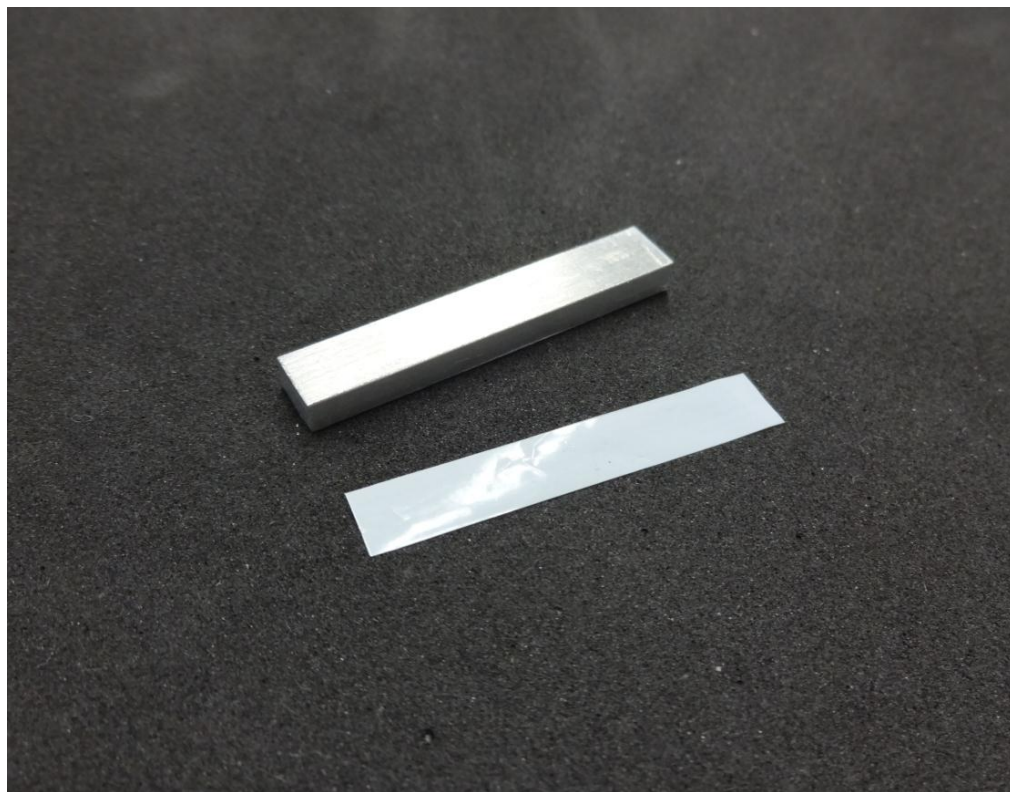
FIGURE 2 CUTTING TEMPLATE POSITIONED NEAR A TESTING SAMPLE

In the first set of experiments, a constant temperature was set to 28.5°C (Room Temperature). The samples were tested in tension at three strain rates: 0.1/s, 0.01/s, and 0.001/s. A 1 gram preload was applied to each sample prior to testing. Because of the anisotropic behavior of the material, the tests were conducted in both the machine and the transverse directions. The deformation of the separator was measured by the DMA and converted to engineering strain defined as:

$$\varepsilon = \frac{\Delta L}{L_o} \tag{1}$$

where ΔL is the elongation of the sample and L_o is the original sample length. Normal axial stress is defined as:

$$\sigma = \frac{F}{A} \tag{2}$$

where F is the measured load delivered by the DMA and A is the cross sectional area of the sample (Callister & Rethwisch, 2010).

For the second set of tests, the temperature chamber was used in order to capture temperature dependence of the separator material. Tensile tests in both the machine

direction and transverse direction were conducted at 55°C and 80°C with a constant strain rate of 0.01/s. The samples were held at the specified temperatures for ten minutes in order to reach equilibrium with the chamber environment. Due to the geometric constrains of the chamber, only about 130% strain was achievable with an initial gauge length of 15mm.
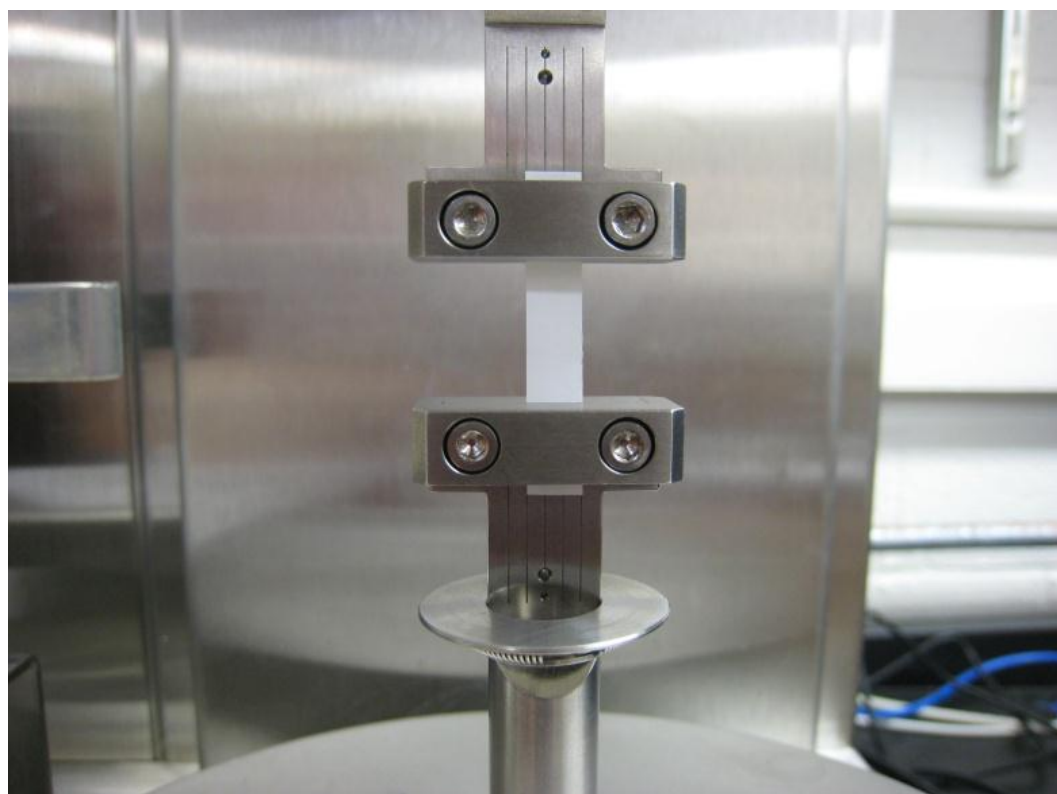
FIGURE 3 DMA TESTING SETUP.

Wet Conditions

A second set of experiments was established in order to determine how the mechanical characteristics of the separator material will change while saturated in a common Lithium ion solvent. The organic solvent, Dimethyl carbonate (DMC), was chosen not only because it is commonly used in Li-ion batteries but because of its classification as a non-volatile organic solvent. The chemical properties of Dimethyl carbonate are shown in Table 2.
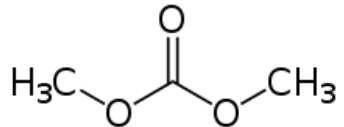
Structural Formula	Molecular Formula	Density (g/cm^3)	Boiling Point (°C)
H_3C—O—C(=O)—O—CH_3	$C_3H_6O_3$	1.07	90

TABLE 2 CHEMICAL PROPERTIES OF DIMETHYL CARBONATE

Dimethyl carbonate can be absorbed through the skin causing inflammation and irritation("Dimethyl Carbonate MSDS," 2011); therefore gloves and goggles were worn at all times while handling the chemical. Additionally due to the high flammability of DMC, the chemical was only exposed to the atmosphere under highly ventilated conditions with no open flames present.

In order to saturate the separator material during testing a special testing fixture was designed. Many testing fixture design iterations (APPENDIX A) were created using Autodesk Inventor® CAD software then printed using a Bits for Bytes® 3D printer to certify its compatibility with the TA RSA III Dynamic Mechanical Analyzer.

The fixture was designed to not only allow the test samples to remain saturated during the testing but to also fit within the temperature chamber. The fixture was made of aluminum due to its ease of milling and corrosion resistance (Figure 4 & Figure 5). The detailed drawings for the fixture are found in APPENDIX A.
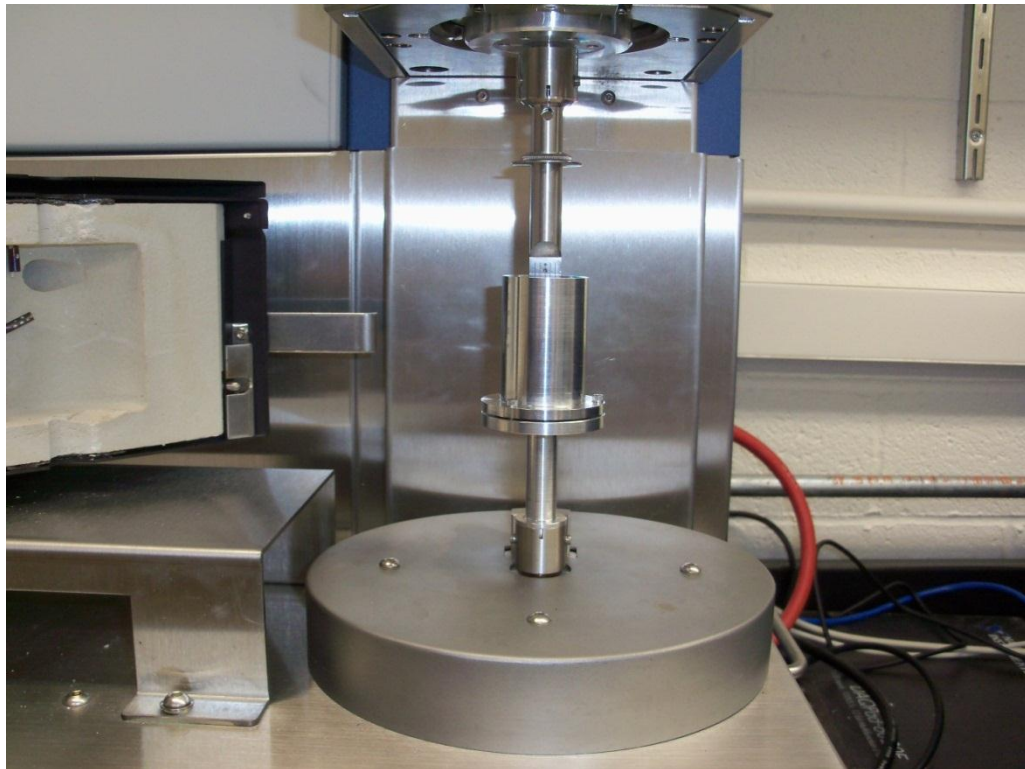
FIGURE 4 TENSILE TESTING FIXTURE WITH SATURATION CHABMER INSTALLED ON TA RSA III DYNAMIC MECHANICAL ANALYZER
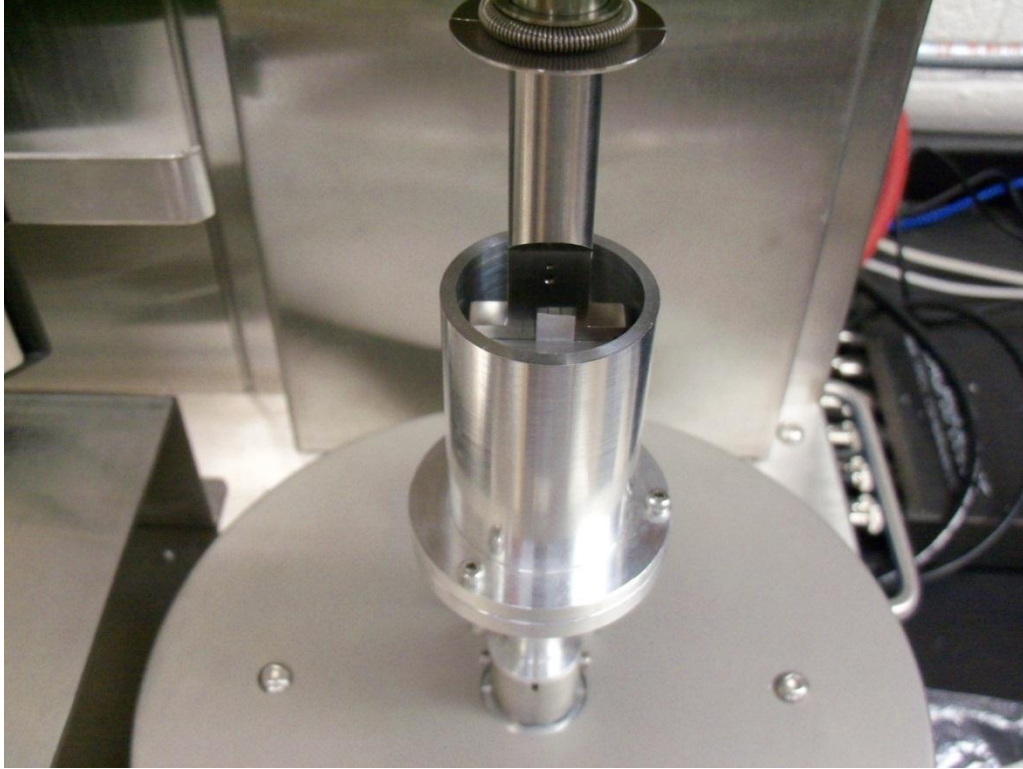
**FIGURE 5 VIEW INTO SATURATION CHAMBER WHERE A SEPARATOR SAMPLE HAS
BEEN CLAMPED**

In order to measure the temperature of the immersion
fluid during testing a FLUKE® Thermometer with a K type
thermocouple was used. The temperature sensor carries a
measurement accuracy of ±0.05% of reading. The sensor was
placed inside the immersion fluid and was strung vertically
along the length of the upper clamp. The heating chamber
was then closed around the fixture and the temperature was
raised. When the Dimethyl carbonate reached the desired
temperature the sensor was removed and the test was
initiated. Removing the sensor is critical in that without

doing so would result in the sensor rubbing against the side of the upper clamp and increasing the forces read by the transducer.

Because of the relatively low vapor pressure of Dimethyl carbonate evaporation happens quickly especially at higher temperatures. This presented a problem when testing at temperatures of 55°C and 80°C where much of the solvent would evaporate during heating and expose the sample to ambient air. In order to reduce the amount of time given for the DMC to evaporate, the solvent was heated prior to its placing in the testing fixture. This was accomplished by heating the DMC with a heated water bath (Figure 6).
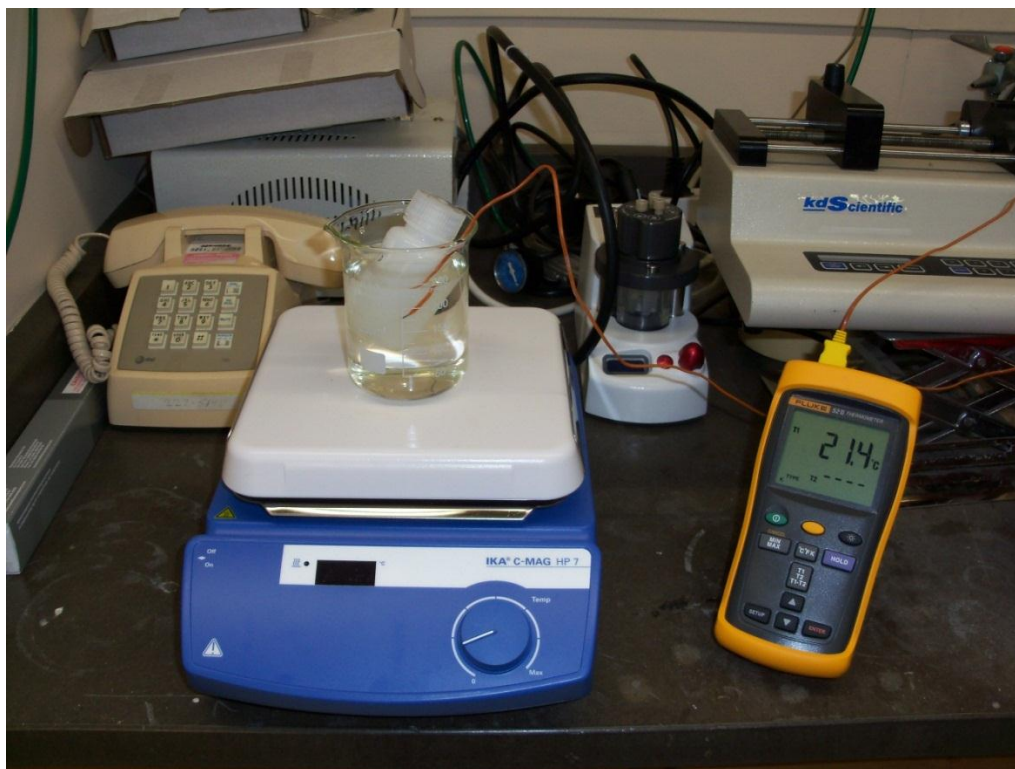
FIGURE 6 EXTERNAL HEATING OF DIMETHYL CARBONATE IN A WATER BATH.

When the DMC reached the desired temperature it was removed from the water bath and placed in the testing fixture. The specified temperature was maintained by the heating chamber for 10 minutes prior to testing.

The saturated condition tests were performed with the same protocol as the dry condition tests. That is samples were tested in both the machine direction and transverse direction at three different strain rates (0.001/s, 0.01/s, 0.1/s) and at three different temperatures (28.5°C, 55°C, and 80°C).

EXPERIMENTAL RESULTS

Dry Testing

For the samples tested in the machine direction, failure sites emerged anywhere between 28% and 48% strain (Figure 7). The linear region can be seen up to about 6% strain with no distinct yield point. The tensile strength of the material reached up to 189 MPa at a strain rate of 0.01/s.
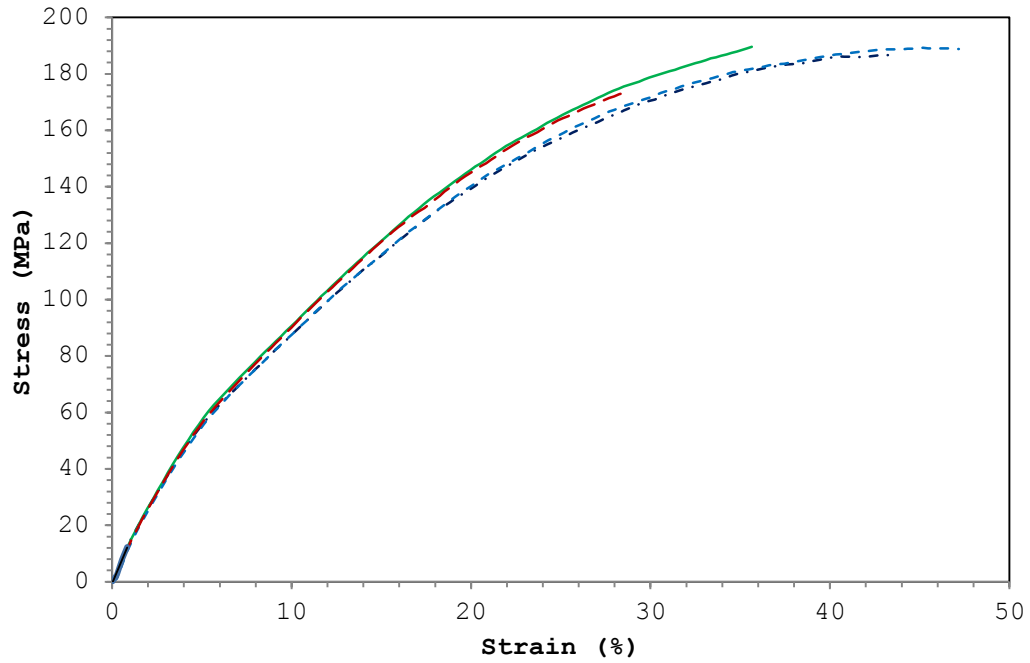
FIGURE 7 STRESS VS. STRAIN AT 28.5°C AND A STRAIN RATE OF 0.01/S (MACHINE DIRECTION).
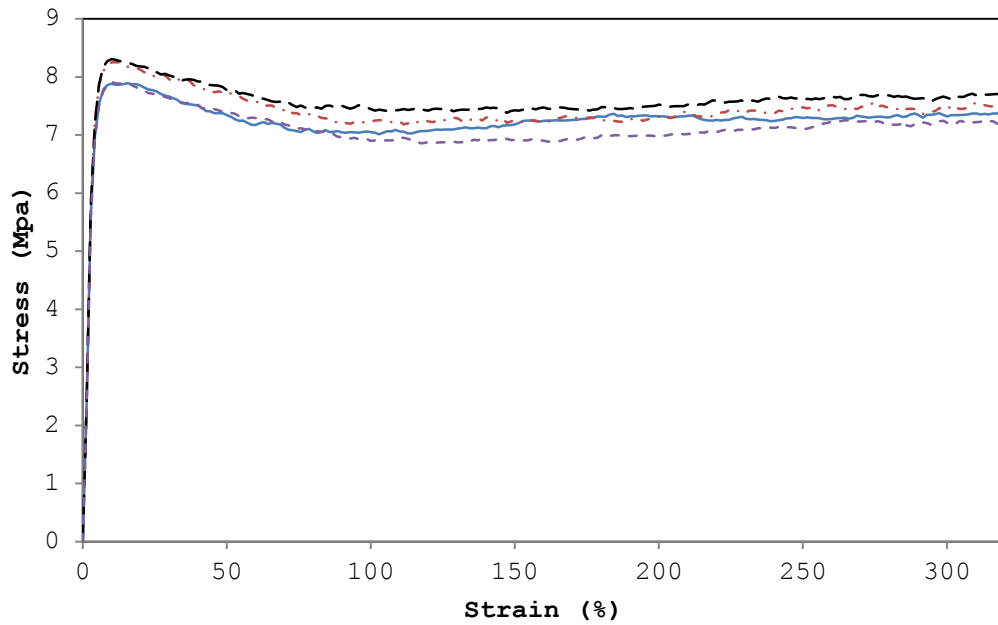
FIGURE 8 STRESS VS. STRAIN AT 28.5°C AND A STRAIN RATE OF 0.01/S (TRANSVERSE DIRECTION).

The transverse direction showed far more distinct elastic and plastic regions in comparison to the machine direction (Figure 8). A linear region was observed up to about 1% strain followed by the onset of yielding. Most samples did not fracture while elongated in the transverse direction and were able to achieve strains of over 400% with a significant decrease in cross sectional area (Figure 9). The stiffness of the separator increased with increasing strain rates in both the machine and transverse directions (Table 3).

Direction	Strain Rate (%)	Young's Modulus (MPa)
Machine	0.1	1071 (±31)
Machine	1.0	1852 (±115)
Machine	10.0	1929 (±-44)
Transverse	0.1	277 (±2.1)
Transverse	1.0	234 (±6)
Transverse	10.0	272 (±8)

TABLE 3   YOUNGS MODULUS OF THE SEPARATOR AT 28.5°C UNDER DRY CONDITIONS

The effect of strain rate on the mechanical response of the material can be easily seen in both the machine and transverse directions (Figure 10 & Figure 11). A significant jump in stress can be seen in the machine direction going from a strain rate of 0.001/s to 0.01/s with only a moderate increase in stress from 0.01/s to 0.1/s. The tensile strength in transverse direction shows linear dependence to the strain rate (Figure 12).

FIGURE 9 SEPARATOR SAMPLE OVEREXTENDED IN TRANSVERSE DIRECTION.
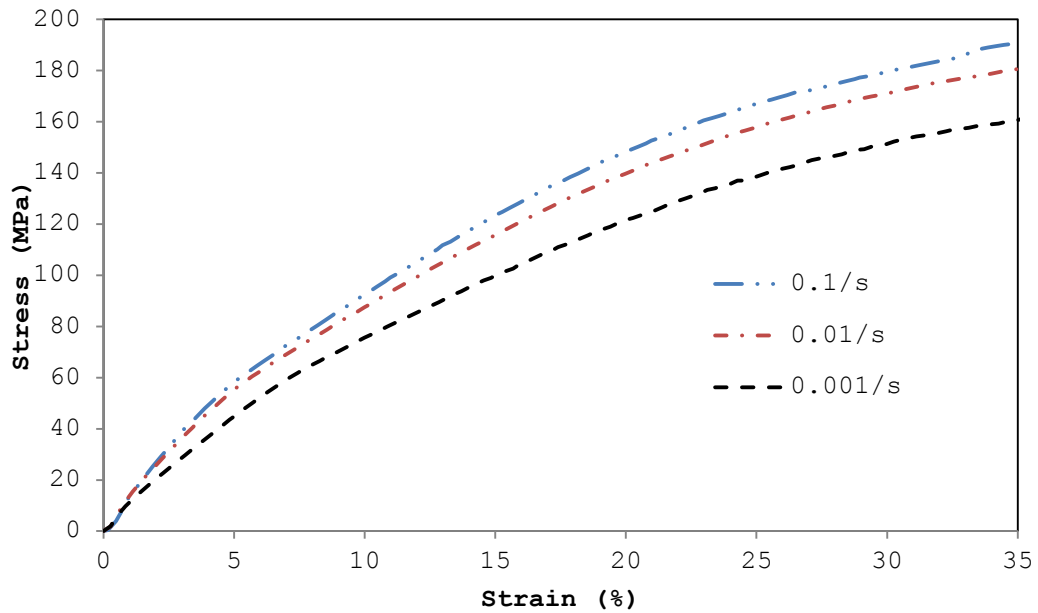
FIGURE 10   COMPARISON OF STRESS/STRAIN CURVES AT DIFFERENT STRAIN RATES (MACHINE DIRECTION).
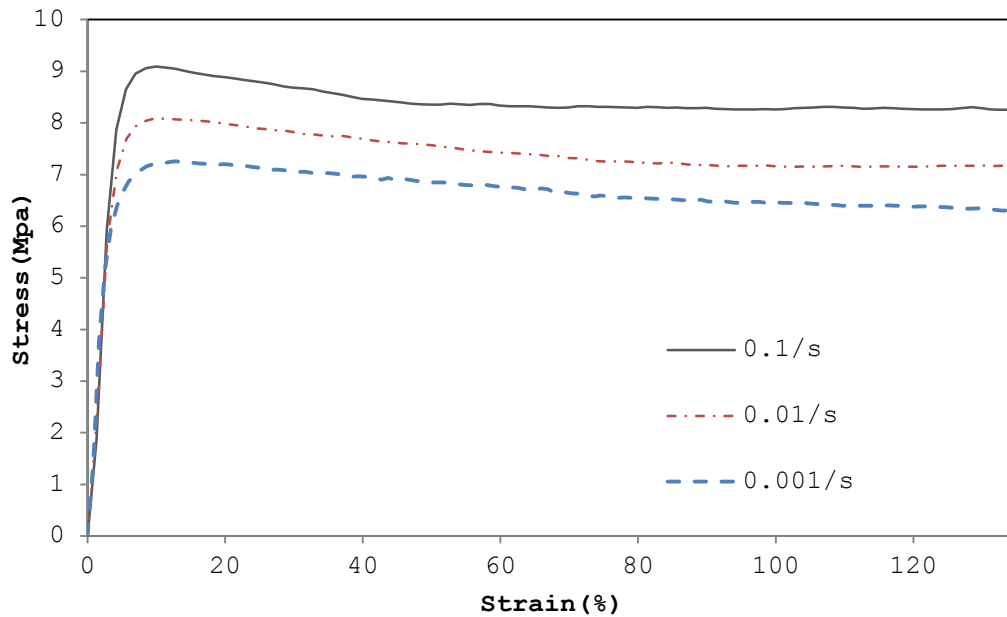
FIGURE 11   COMPARISON OF STRESS/STRAIN CURVES AT DIFFERENT STRAIN RATES (TRANSVERSE DIRECTION).
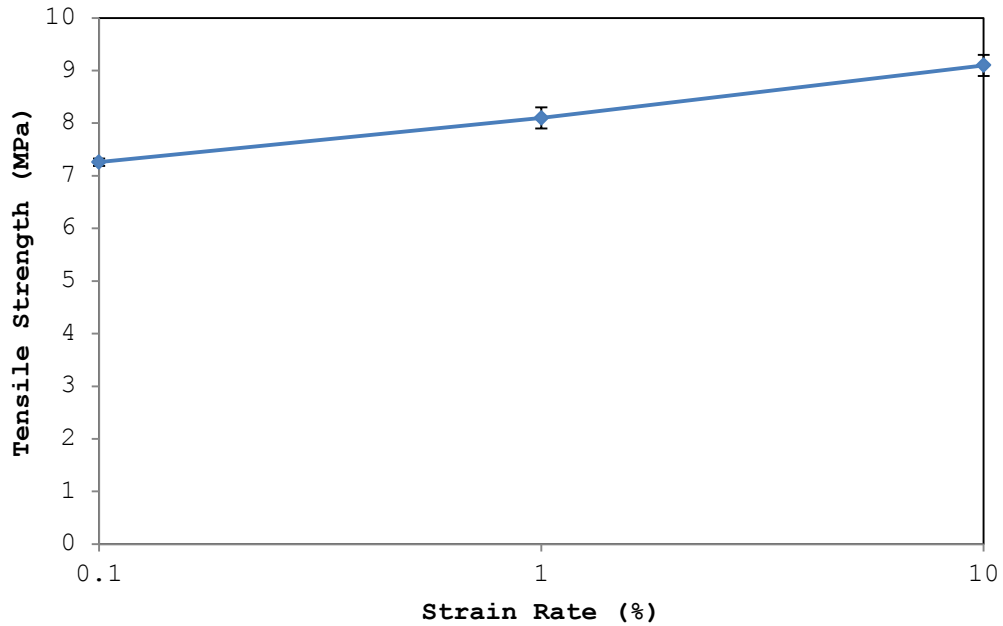
FIGURE 12   EFFECT OF STRAIN RATE ON TENSILE STRENGTH IN THE TRANSVERSE DIRECTION.

The separator material exhibited strong temperature dependence, with a significant decrease in yield stress for higher temperatures (Figure 13 & Figure 14). Testing in both the machine and transverse direction shows that an increase in temperature induces a nearly linear decrease in the tensile strength of the material (Figure 15). For each of the test conducted in the transverse direction a standard deviation of <.22 was calculated for the tensile strength.

Additionally the stiffness of the material decreased with increasing temperature in both the machine and transverse directions (Table 4).
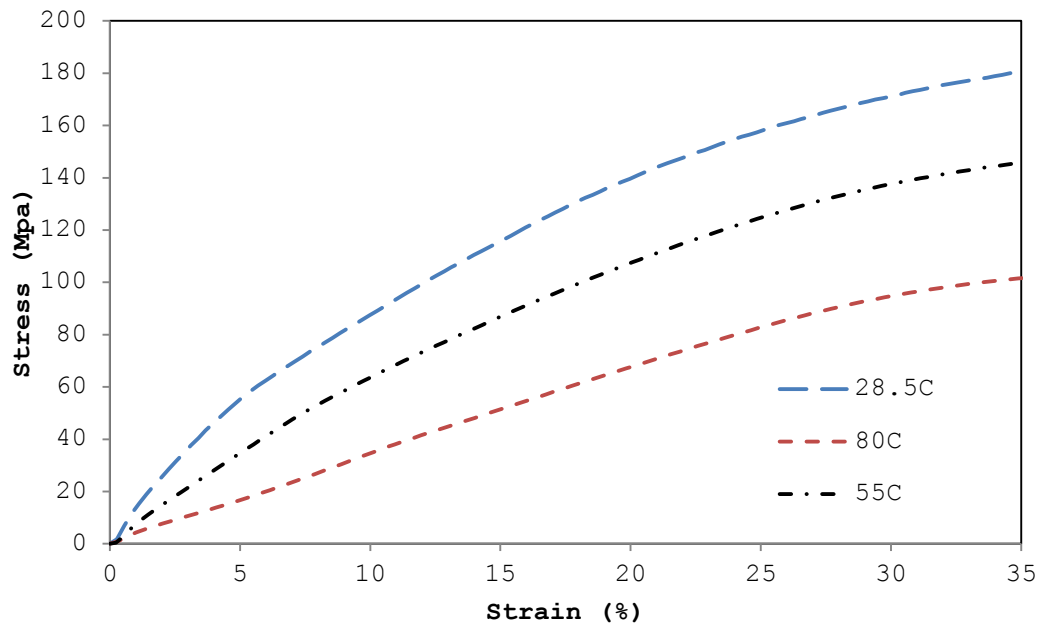
FIGURE 13   COMPARISON OF STRESS VS. STRAIN CURVES AT DIFFERENT TEMPERATURES (MACHINE DIRECTION).
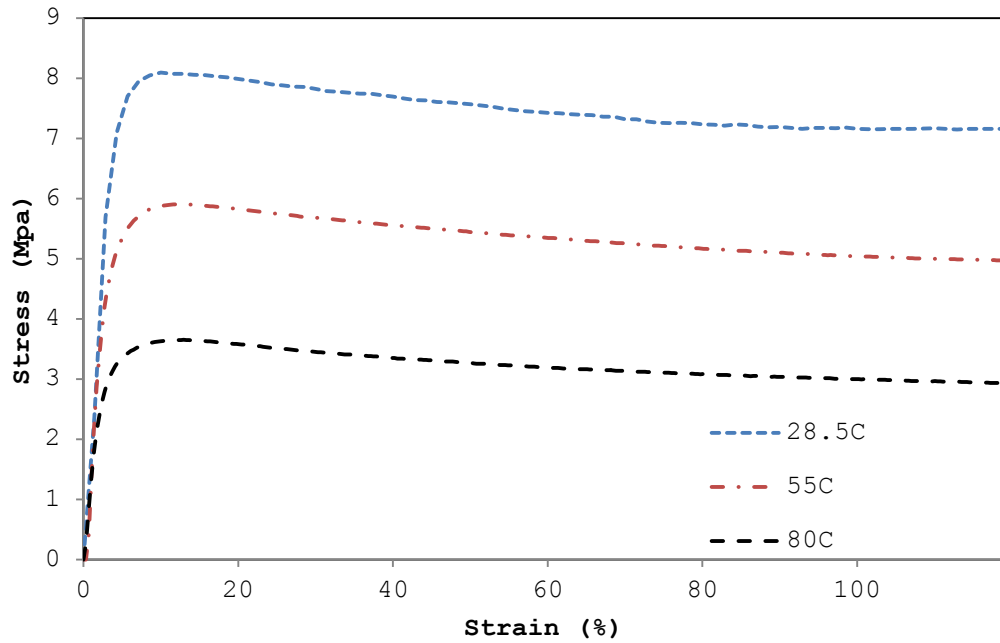
FIGURE 14   COMPARISON OF STRESS VS. STRAIN CURVES AT DIFFERENT
TEMPERATURES (TRANSVERSE DIRECTION).
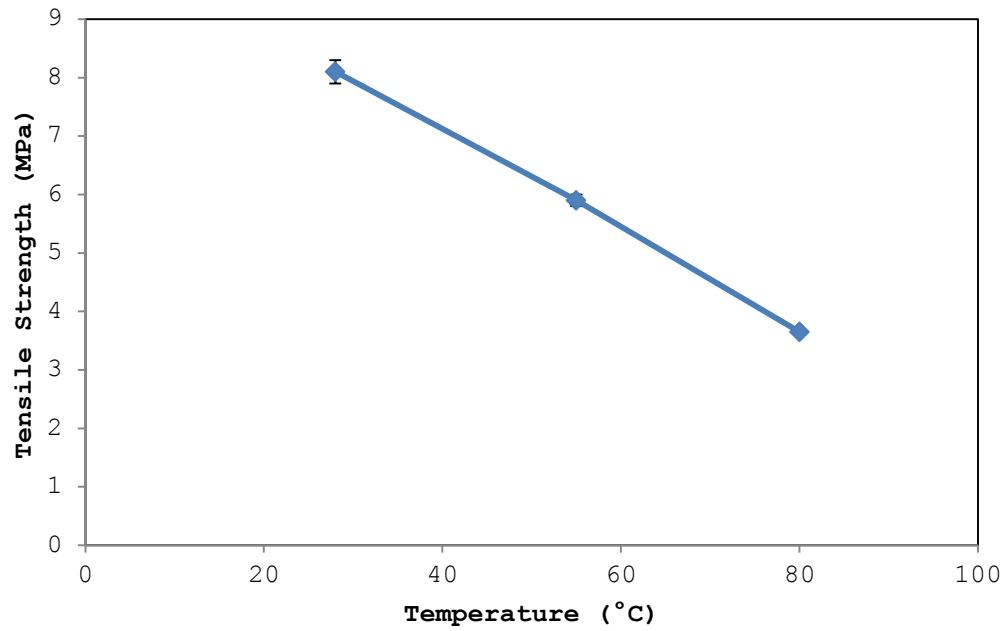
FIGURE 15   DEPENDANCE OF TENSILE STRENGTH TO TEMPERATURE IN TRANSVERSE
DIRECTION, STRAIN RATE = 1.0%.

Direction	Temperature (°C)	Young's Modulus (MPa)
Machine	28.5	1852 ±115
Machine	55	1054 ±70
Machine	80	537 ±39
Transverse	28.5	310 ±8
Transverse	55	215 ±8
Transverse	80	129 ±15

TABLE 4 YOUNG'S MODULUS FOR MACHINE AND TRANSVERSE DIRECTIONS AT VARIED TEMPERATURES.

Wet Testing

The shape of the stress vs. strain curves for Celgard C480 separator saturated with DMC is similar to that seen during dry testing. An increase in the strain rate for both the machine direction and the transverse direction resulted in an increase in material strength as can be seen in Figure 16 & Figure 17. Increasing the strain rate also led to an increase in stiffness shown in Table 5. Additionally, raising the temperature had a negative effect on the strength for samples in the machine direction and transverse direction (Figure 18 & Figure 19). Similarly, a decrease in temperature resulted in an increase in

stiffness as shown in Table 6. A linear relationship can be seen between tensile strength and strain rate (Figure 20). Likewise, this same linear relationship can be seen between tensile strength and temperature (Figure 21).

Direction	Strain Rate (%)	Modulus (MPa)
Machine	0.1	1071 ±31
Machine	1	1123 ±169
Machine	10	1135 ±31
Transverse	0.1	269 ±45
Transverse	1	310 ±8
Transverse	10	401 ±46

TABLE 5 LIST OF YOUNG'S MODULUS AT DIFFERENT STRAIN RATES FOR MACHINE AND TRANSVERSE DIRECTIONS.

Direction	Temperature (°C)	Modulus (MPa)
Machine	28.5	1123 ±169
Machine	55	730 ±25
Machine	80	289 ±11
Transverse	28.5	310 ±8
Transverse	55	215 ±8
Transverse	80	129 ±15

TABLE 6 LIST OF YOUNG'S MODULUS AT DIFFERENT TEMPERATURES FOR MACHINE AND TRANSVERSE DIRECTIONS.
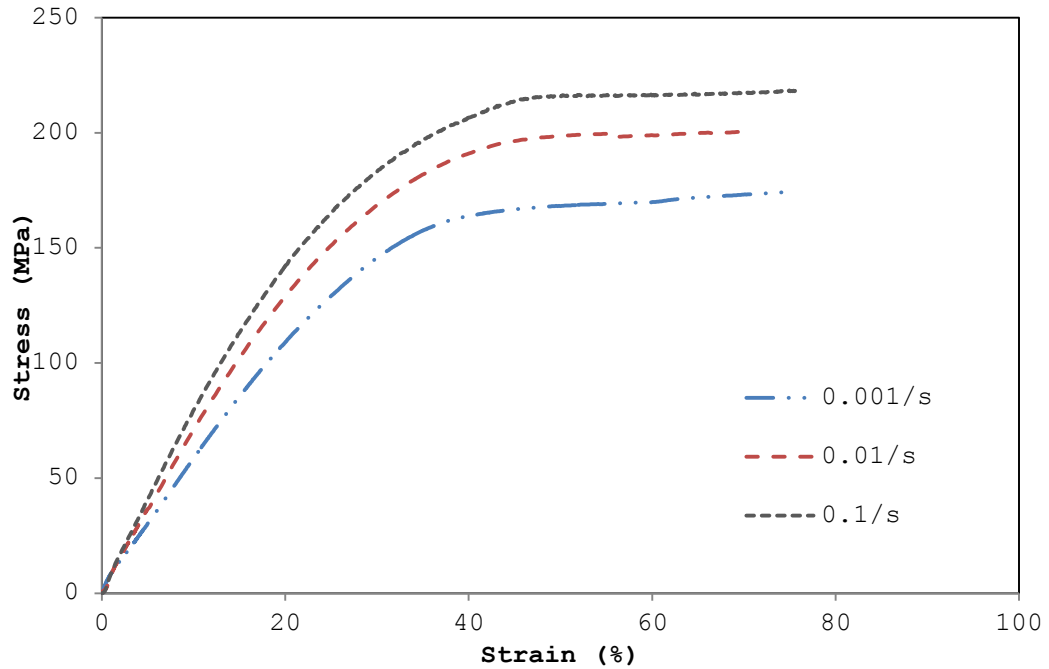
FIGURE 16 COMPARISON OF STRESS VS. STRAIN AT DIFFERENT STRAIN RATES
WHILE SATURATED AT 28.5°C (MACHINE DIRECTION).
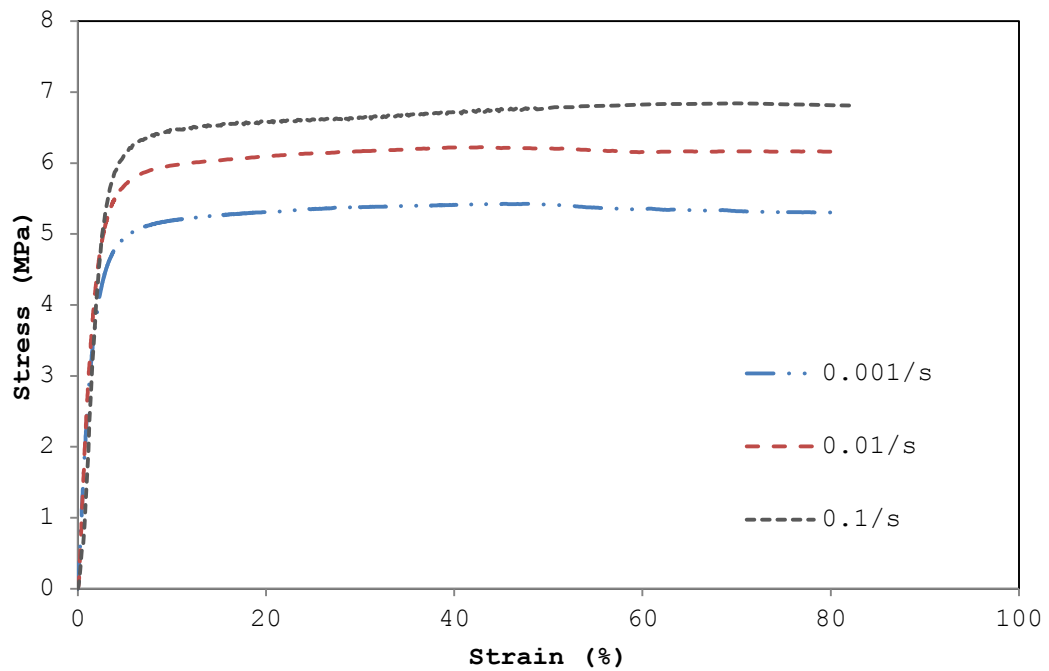
FIGURE 17 COMPARISON OF STRESS VS. STRAIN AT DIFFERENT STRAIN RATES
WHILE SATURATED AT 28.5°C (TRANSVERSE DIRECTION).
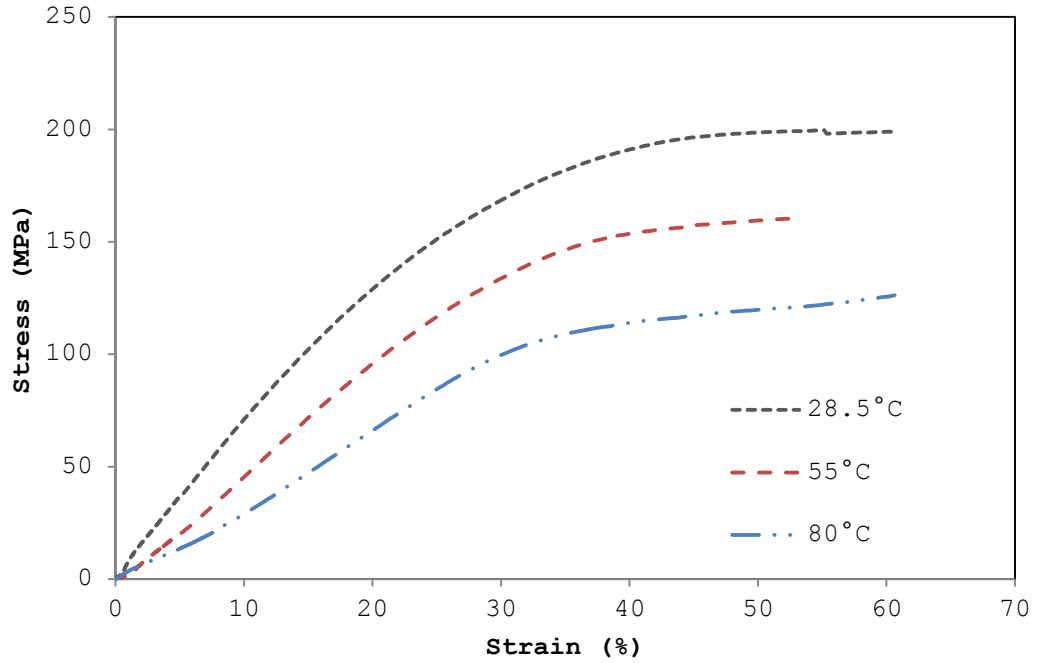
FIGURE 18 COMPARISON OF STRESS VS. STRAIN AT DIFFERENT TEMPERATURES
WHILE SATURATED. STRAIN RATE SET AT 0.01/S (MACHINE DIRECTION).
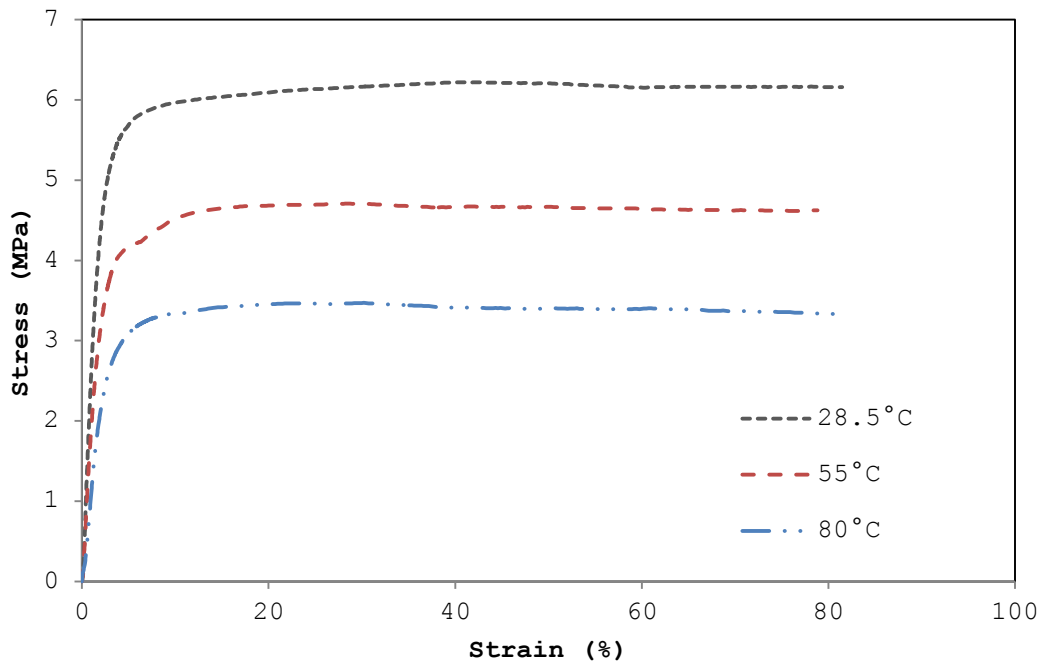
FIGURE 19 COMPARISON OF STRESS VS. STRAIN AT DIFFERENT TEMPERATURES
WHILE SATURATED WITH STRAIN RATE SET AT 0.01/S (TRANSVERSE DIRECTION).
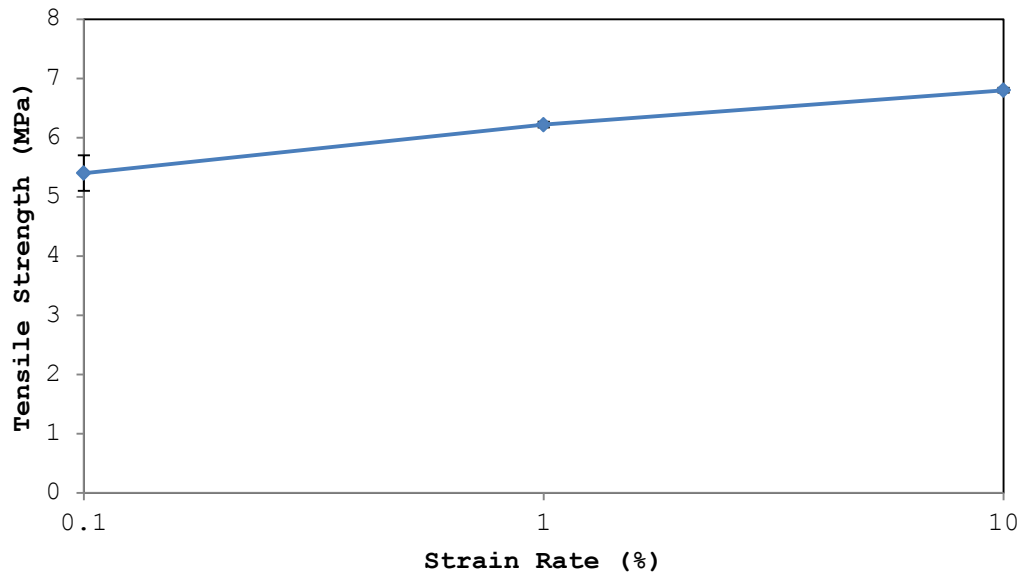
FIGURE 20 DEPENDANCE OF TENSILE STRENGTH TO STRAIN RATE WHILE SATURATED, TEMPERATURE AT 28.5°C (TRANSVERSE DIRECTION).
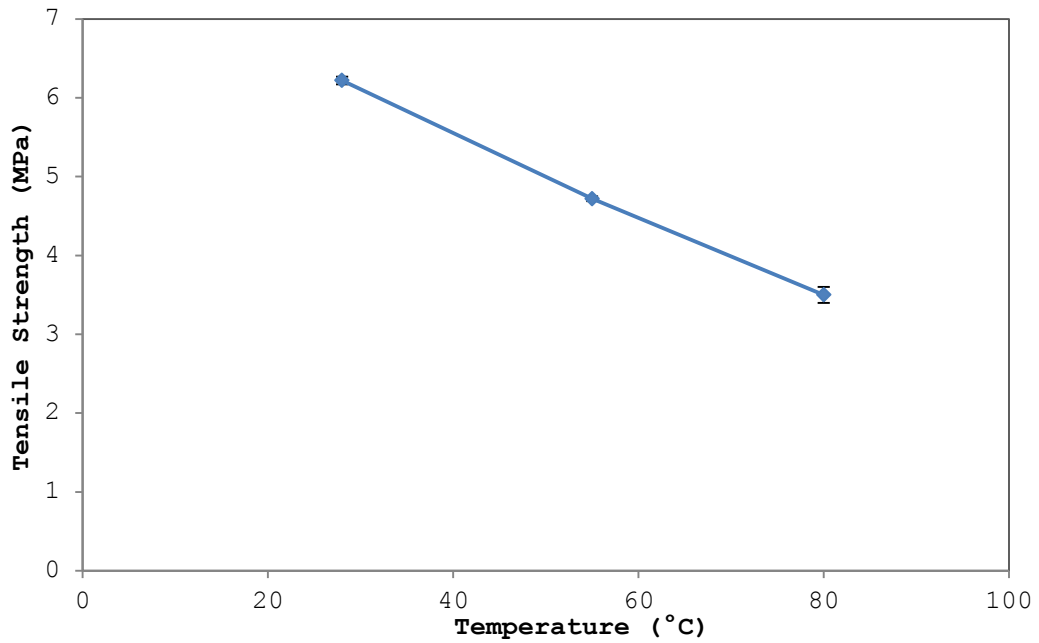
FIGURE 21 DEPENDANCE OF TENSILE STRENGTH TO TEMPERATURE WHILE SATURATED, STRAIN RATE AT 0.01/S (TRANSVERSE DIRECTION)

Comparison of Experimental Results

Compared to dry testing of the separator material, saturated samples displayed an increase in compliance in the machine direction during all tests. This can be seen as the elastic stiffness and yield stress decrease with the introduction of the solvent. The toughness of the material in the machine direction also increased when saturated in DMC. At a strain rate of 0.001/s the tensile strength for both the saturated and dry samples leveled out at nearly 160MPa (Figure 40). At higher strain rates the tensile strength of the saturated material surpassed that of the dry samples. As can be seen in Figure 41 and Figure 42 increasing the strain rate increases the magnitude of the difference in tensile strength between saturated and dry samples.

For samples loaded in the transverse direction the initial stiffness of the material remains relatively similar for saturated and dry samples (Figure 43, Figure 44, Figure 45). The onset of yielding occurs significantly sooner for saturated samples with the tensile strength falling nearly 2.5 MPa lower than that of dry samples. The shape of the stress strain curve is also altered when samples are saturated in DMA in that stress values for wet samples

quickly plateau after yielding and maintain values near their tensile strength. This is in contrast to dry samples which when stressed to their ultimate tensile strength quickly soften. As with samples loaded in the machine direction; an increase in strain rate results in heightened stiffness and tensile strength for both saturated and dry samples.

Temperature also plays a critical role in the mechanical characteristics of the separator material. For samples loaded in the machine direction, saturated samples showed an increase in compliance in both at all temperatures in comparison to dry samples (Figure 46, Figure 47, Figure 48). As temperatures increased from 28.5°C to 80° the tensile strength of the saturated materials began to surpass those of dry samples at lower strains. Likewise, for samples loaded in the transverse direction as temperatures increased the tensile strength of both dry and wet samples increased in similarity (Figure 49, Figure 50, & Figure 51). The trend suggests that temperature has a greater effect on the tensile strength of the material, regardless of direction, than saturation.

CONSTITUTIVE MODELING

Bergstrom Hybrid Constitutive Model

The hybrid constitutive model, developed by Bergstrom and coworkers was developed to simulate the mechanical properties of ultra-high molecular weight polyethylene (UHMWPE) at large strain rates (Bergström et al., 2002) but can be applied to many types of thermoplastics. The model can be represented as series of springs and dashpots (Figure 22) with the spring **E** representing the linear elastic region, dashpot **P** representative of the materials viscoplastic region, and back stress components labeled **A** and **B** (Bowden, Oneida, & Bergstr, n.d.).
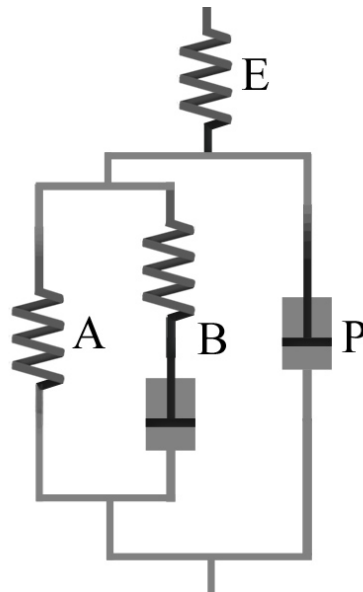
FIGURE 22 RHEOLOGICAL REPRESENTATION OF THE HYBRID MODEL.

The model homogenizes the amorphous and crystalline microstructure of the polymer and describes its mechanical properties in terms of elastic and viscoplastic deformation:

$$F = F^e F^p \tag{3}$$

where F is the applied deformation gradient and F^e and F^p represent the elastic and plastic components respectively. The Cauchy stress at a given deformation state in the elastic region is given by:

$$T^e = \frac{1}{J^e}(2\mu E^e + \lambda tr[E^e]I) \tag{4}$$

The left stretch tensor is given as V^e which is used to determine the logarithmic true strain $\mathbf{E^e} = \ln[\mathbf{V^e}]$. The relative elastic volume change can be computed as $\mathbf{J^e} = \det[\mathbf{F^e}]$, and μ^e, λ^e are Lame's constants which can be derived from the Young's modulus ($\mathbf{E}$) and the poisons ratio ($\boldsymbol{v}$) using equations:

$$\mu = \frac{E}{2(1+v)} \tag{5}$$

$$\lambda = \frac{Ev}{(1+v)(1-2v)} \tag{6}$$

The influence of the crystalline phase on the rearrangement of the amorphous phase and deformation resistance can be modeled by combining a non-linear behavior containing a

shear modulus dependant on the local strain with the Arruda-Boyce 8 chain model, given as:

$$T^p = \left\{ \frac{E_f \varepsilon - \hat{\varepsilon}(E_i - E_f)[e^{-\frac{\varepsilon}{\hat{\varepsilon}}} - 1]}{e^{2\varepsilon} - e^{-\varepsilon}} + \frac{\mu^p}{\overline{\lambda^p}} \frac{L^{-1}\left(\frac{\overline{\lambda^p}}{\lambda_{lock}^p}\right)}{L^{-1}\left(\frac{1}{\lambda_{lock}^p}\right)} \right\} dev[\mathbf{B}^p] \tag{7}$$

Where E_f, E_i, and $\hat{\varepsilon}_1$ are material parameters concerning the non-linear elastic character of the crystalline phase, the effective strain is defined as $\varepsilon = \sqrt{\frac{2}{3}} \|E^p\|_F$, μ^p and λ_{lock}^p is the shear modulus locking chain stretch of the back stress network. The effective chain stretch of the back stress network given as $\overline{\lambda^p} = \sqrt{tr[B^p]/3}$, where B^p is the distortional portion of the left Cauchy Green tensor of the back stress network given as $B^p = F^p F^{pT}$. The stress driving the plastic deformation can then be calculated by subtracting the back stress from the total stress as follows:

$$T^* = T - \frac{1}{J^e} F^e T^p F^{eT} \tag{8}$$

The power rule is used to incorporate the evolution and distribution of activation energies with the following equation:

$$\dot{\gamma}^p = \left(\frac{\tau}{\tau_{base}}\right)^{m(\varepsilon)} \tag{9}$$

Where τ is the shear stress and τ_{base} is the reference shear stress. The stress exponent m changes with strain and is given by;

$$m(\varepsilon) = \left\{ m_f + (m_i - m_f)\left[1 - \frac{\varepsilon}{\widehat{\varepsilon_2}}\right]^{\alpha}, if\ \varepsilon < \widehat{\varepsilon_2},\ m_f\ otherwise \right. \tag{10}$$
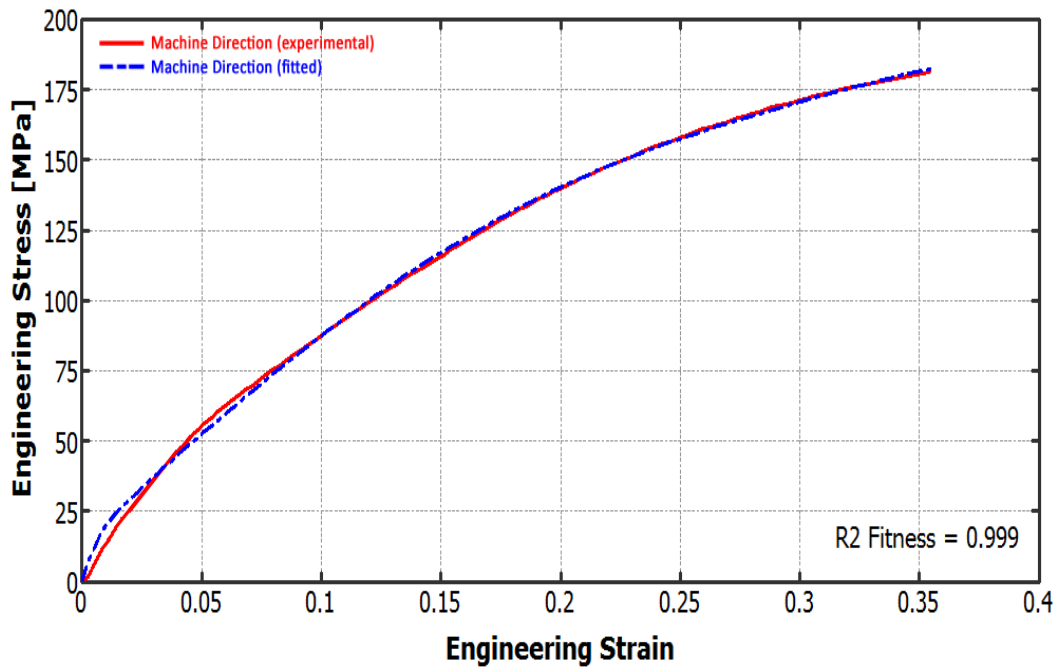
FIGURE 23 STRESS/STRAIN CURVE FIT USING HYBRID BERGSTROM MODEL (MACHINE DIRECTION).
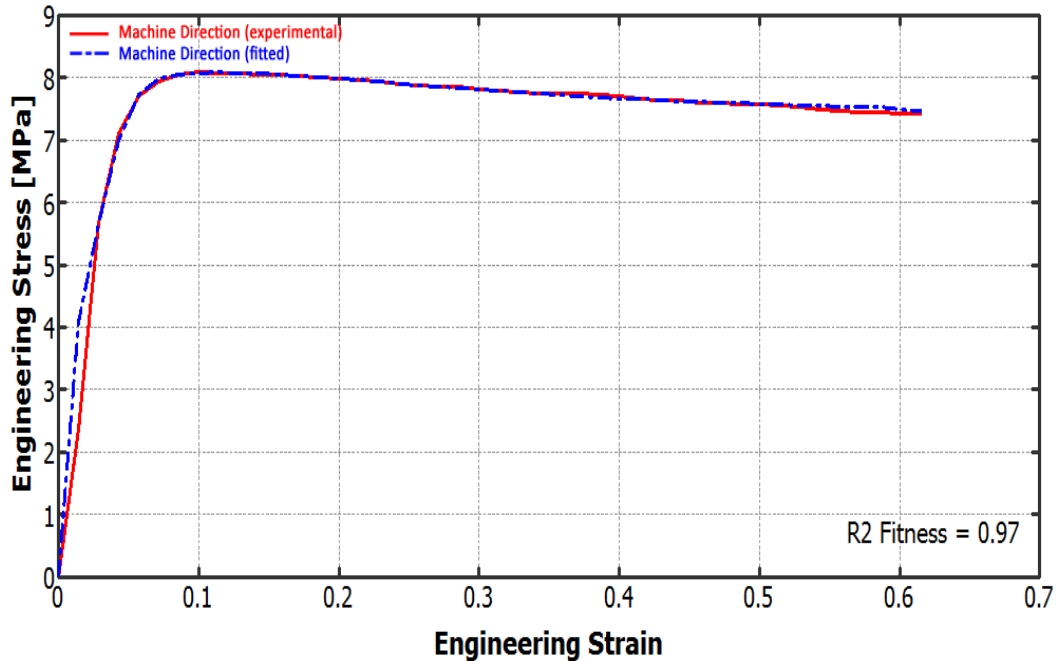
FIGURE 24 STRESS/STRAIN CURVE FIT USING HYBRID BERGSTROM MODEL (TRANSVERSE DIRECTION).

Each of the simulations were solved using MCallibration® software which utilizes a series of optimization methods to determine the best fit of parameter constants associated with a chosen material model. The 14 optimized parameters for the Hybrid Model can be seen in Table 7 for both the machine and transverse directions.

The hybrid Bergstrom model has shown to be effective in modeling the mechanical response of the battery separator in both the machine and transverse direction (Figure 23 & Figure 24). The greatest deviation of the fitted material response was found in modeling the transverse direction with only a slight mismatch in capturing the onset of

yielding. The shortcoming of the model is that it can only follow the behavior of isotropic materials.

An additional feature of the MCalibration® Advanced Material Modeling software is the generation of program code of the material model's simulation that can be directly imported into ANSYS, Abaqus, or LS-DYNA. The APDL code for ANSYS multiphysics simulation software of the Hybrid model and its optimized parameters for both the machine and transverse directions can be found in APPENDIX C.

Parameter	Description	Machine Direction Value	Transverse Direction Value
E	Young's modulus	2560.58	456.29
v	Poisson's ratio	0.5	0.46
μ_A	Shear modulus	170.03	2.14
λ_L	Locking stretch	5.13	2.76
q	Relative contribution of l_2 of network A	0	0.01
K	Bulk Modulus	96131.1	1762.67
S_{bi}	Initial Stiffness B	31.83	40.60
S_{bf}	Final Stiffness B	1.47	27.13
α_B	Transition rate stiffness B	21122.1	17.48
T_{base}^{B}	Flow resistance B	292.61	7.69
m_B	Stress exponent B	3.49	14.2
$\hat{P}$	Pressure dependence flow	906.69	70.51
T_{base}^{P}	Flow resistance p	133.1	2.80
m_P	Stress exponent p	2.29	4.97

TABLE 7 OPTIMIZED MATERIAL PARAMETERS FOR HYBRID MODEL

Anisotropic Bergstrom-Boyce Model

The Bergstrom-Boyce model was developed to predict the time-dependent, large-strain behavior of elastomer-like materials (*PolyUMod; A Library of Advanced User Materials*, n.d.). The model is an extension of the Arruda-Boyce eight chain model (Arruda & Boyce, 1993).

The stress response of the Arruda-Boyce model is given as:

$$\sigma = \frac{\mu}{J\bar{\lambda}^*} \frac{\mathcal{L}^{-1}(\frac{\bar{\lambda}^*}{\lambda_L})}{\mathcal{L}^{-1}(\frac{1}{\lambda_L})} \mathrm{dev}[b^*] + k(J-1)I \tag{11}$$

Where the shear modulus is given as μ, bulk modulus is k

$$\tag{12}$$

and the limiting chain stretch is λ_L. The distortional left Cauchy-Green tensor is described as:

$$b^* = J^{-2/3}b$$

The applied chain stretch $\bar{\lambda}^*$ is given as:

$$\bar{\lambda}^* = \sqrt{\frac{\mathrm{tr}[b^*]}{3}} \tag{13}$$

The Langevian function $\mathcal{L}(x) = \coth(x) - 1/x$ is inverted to give $\mathcal{L}^{-1}(x)$ and can be approximated from (Bergstrom, 1999):

$$\mathcal{L}^{-1} \approx \begin{cases} 1.31146 \tan(158968x) + 0.91209x, & \text{if } |x| < 0.84137 \\ \frac{1}{\mathrm{sgn}(x) - x}, & \text{if } 0.84136 \leq |x| < 1. \end{cases} \tag{14}$$

For the Bergstrom-Boyce model, the deformation gradient can be described as two macromolecular networks in parallel. A rheological expression of this relationship is shown in Figure 25. Where the deformation gradient acting on the two networks is :

$$F = F_A = F_B \tag{15}$$

The non-linear network B can be further broken down into both elastic and visco-elastic components represented as:

$$F = F_B^e F_B^v \tag{16}$$
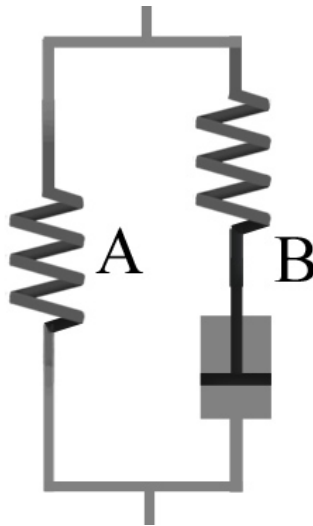
FIGURE 25 RHEOLOGICAL EXPRESSIION OF THE BERGSTROM BOYCE MODEL

The stress response in network A and B is given by the Arruda-Boyce eight chain model with network B carrying a different effective shear modulus:

$$\sigma_A = \frac{\mu}{J\overline{\lambda}^*}\frac{\mathcal{L}^{-1}(\frac{\overline{\lambda}^*}{\lambda_L})}{\mathcal{L}^{-1}(\frac{1}{\lambda_L})}\mathrm{dev}[b^*] + k(J-1)\boldsymbol{I} \qquad (17)$$

$$\sigma_B = \frac{s\mu}{J_B^e\overline{\lambda}_B^{e*}}\frac{\mathcal{L}^{-1}(\frac{\overline{\lambda}_B^{e*}}{\lambda_L})}{\mathcal{L}^{-1}(\frac{1}{\lambda_L})}\mathrm{dev}[b_B^{e*}] + k(J_B^e-1)\boldsymbol{I} \qquad (18)$$

Where the shear modulus of network B in relation to network A is given as the dimensionless parameter s, and the chain stretch in the elastic portion of network B is $\overline{\lambda}_B^{e*}$. The total Cauchy stress is then given as:

$$\sigma = \sigma_A + \sigma_B \qquad (19)$$

In order to model the anisotropic behavior of a material an additional anisotropic stress term is added to both network (20) A and B:

$$\sigma_A = \sigma_{8chain}(\mathrm{F}) + \left[A_f\lambda_f^2 + B_f\lambda_f - (A_f + B_f)\right]a_f\otimes a_f,$$

$$\sigma_B = \sigma_{8chain}(\mathrm{F}_B^e) + \left[A_f(\lambda_{fB}^e)^2 + B_f\lambda_{fB}^e - (A_f + B_f)\right]a_{fB}^e\otimes a_{fB}^e, \qquad (21)$$

Where the Arruda-Boyce 8 chain model is denoted as σ_{8chain}, $a_f = F_{a_0}$, $\widehat{a_f} = \mathrm{F}_{a_0}/\lambda_f$, $\lambda_f = \|a_f\|$, $\hat{a}_{fB}^e = F_B^e a_0/\lambda_{fB}^e$, and $\lambda_{fB}^e = \|a_{fB}^e\|$ (*PolyUMod; A Library of Advanced User Materials*, n.d.)

The MCalibration® Software comes with a variety of advanced material models including the option of combining material models in parallel known as the Parallel Network Model. To model the anisotropic behavior of the battery

separator the anisotropic Bergstrom-Boyce model was combined with neo-hookean hyper elastic model where the Cauchy stress is given as:

$$\sigma = \frac{\mu}{J}\text{dev}[b^*] + k(J-1)I \tag{22}$$

An exponential yield evolution factor $f_{\varepsilon p}$ is also added to the network and is given as:

$$f_{\varepsilon p} = f_f + (1-f_f)exp\left[\frac{-\varepsilon_p}{\hat{\varepsilon}}\right] \tag{23}$$

Where the resistance in the model grows with the increase in Mises plastic strain shown as:

$$\varepsilon_p = \sqrt{\frac{2}{9}\left[(\varepsilon_1^v - \varepsilon_2^v)^2 + (\varepsilon_2^v - \varepsilon_3^v)^2 + (\varepsilon_3^v - \varepsilon_1^v)^2\right]} \tag{24}$$

To assemble the model in Mcalibration® the parallel network model must be chosen and the additional models selected as shown in FIGURE 26. The model was successfully able to predict the stress vs. strain curves in both the machine direction and transverse direction carried an r^2 fitness value of 0.963 (Figure 27). The greatest fit of the stress vs. strain curve was found in the machine direction (Figure 28) where only a small deviation occurred after the onset of yielding. A less accurate prediction occurred in the fitting of the stress vs. strain curve in the transverse direction (Figure 29) where the model predicted

a significantly stiffer elastic region and an early onset of yielding. The material constants for the model are given in Table 8. Additionally, the APDL code of the material model for ANSYS® multiphysics simulation software is given in APPENDIX C.
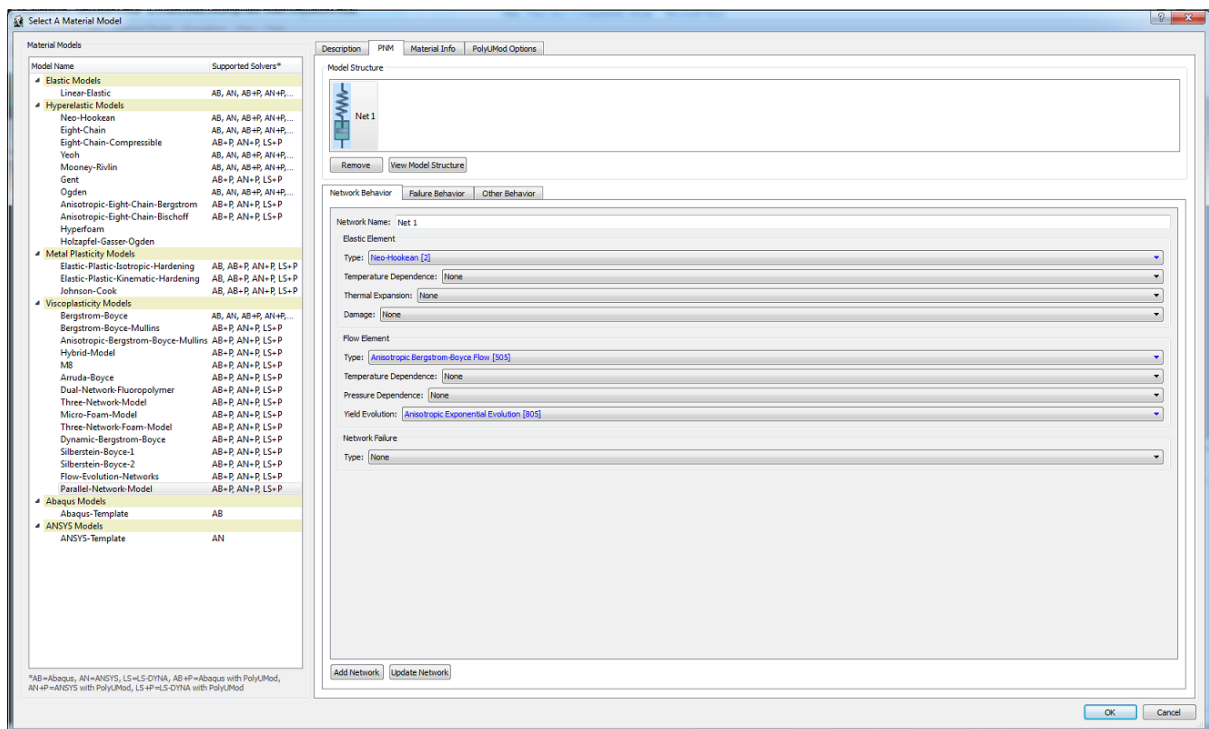
FIGURE 26 MCALIBRATION PARALLEL NETWORK MODEL SELECTION GUI
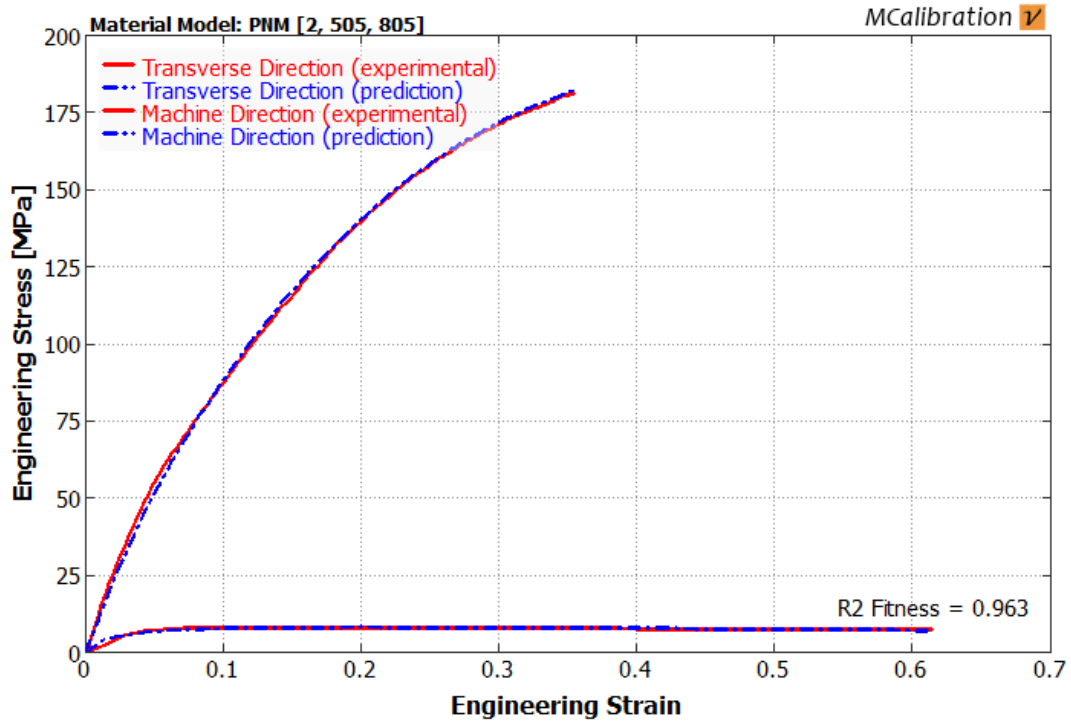
FIGURE 27 ANISOTROPIC BERGSTROM-BOYCE MODEL PREDICTION IN MD & TD
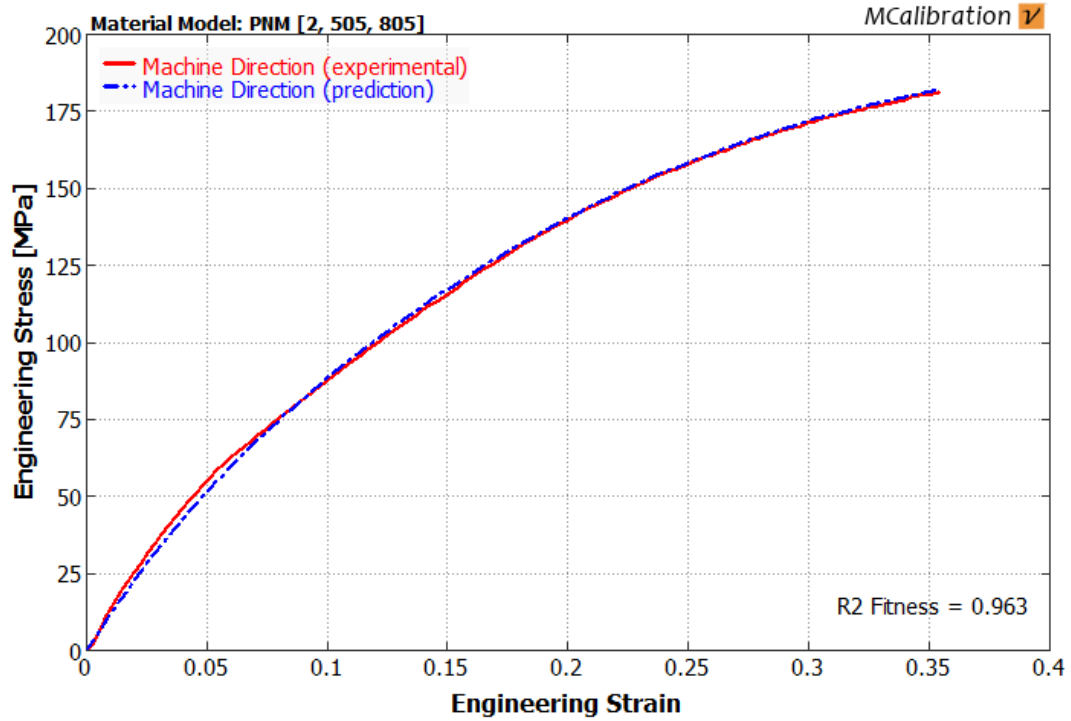
FIGURE 28 ANISOTROPIC BERGSTROM-BOYCE MODEL PREDICTION IN THE MACHINE DIRECTION
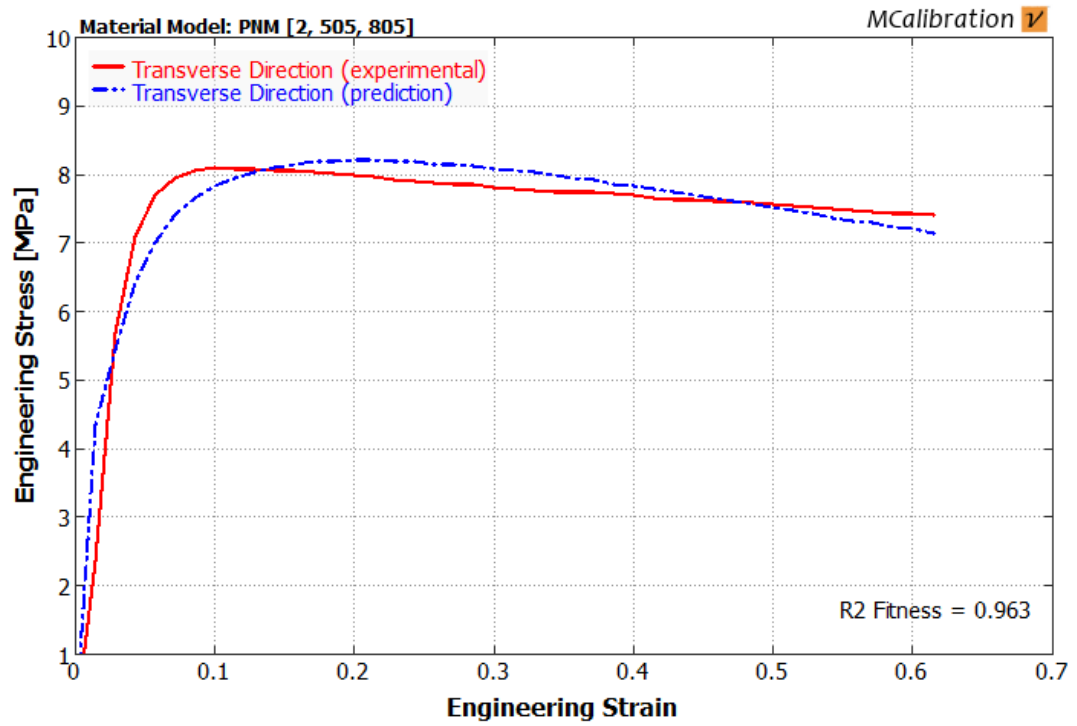
FIGURE 29 ANISOTROPIC BERGSTROM-BOYCE MODEL PREDICTION IN THE TRANSVERSE DIRECTION

Parameter	Description	Value
μ	Shear modulus of network A	485.985
K	Bulk Modulus	710.554
ξ	Strain adjustment factor	4.107e-80
C	Strain exponential	-.524
$\hat{\tau}$	Flow resistance	77.296
m	Stress exponent	5
F	Hill Parameter F	30.5
G	Hill Parameter G	0.01868
H	Hill Parameter H	0.01868
L	Hill Parameter L	3.13809
M	Hill Parameter M	2.296
N	Hill Parameter N	3.255
f_f	Final value of $f_{\varepsilon p}$	2.034
$\hat{\varepsilon}$	Characteristic transition strain	0.091397

TABLE 8 OPTIMIZED PARAMETERS FOR THE ANISOTROPIC BERGSTROM-BOYCE MODEL

CONCLUSION

In this body of work a number of key benchmarks were reached including:

1. Tensile testing of a lithium-ion battery separator in both its machine and transverse direction.

2. Determination of the mechanical properties of a lithium-ion battery separator under tension at varying strain rates and temperatures.

3. Design and development of a tensile testing fixture capable of saturating a thin polymer film at elevated temperatures.

4. Determination of the mechanical properties of a lithium-ion battery separator, saturated in a common organic solvent, under tension at varying strain rates and temperatures.

5. Application of both an isotropic and anisotropic constitutive model to predict the stress vs. strain characteristics of a battery separator in tension.

A polymer CELGARD C480 Lithium-ion battery separator was tested in tension with a dynamic mechanical analyzer. The mechanical properties of the material have been proven to be dependent upon strain rate, temperature, and saturation in an organic solvent. Furthermore an increase in the

strain rate induces a linear strengthening effect on the material in both the machine and transverse directions. The mechanical properties of the separator are also largely dependent upon temperature where an increase in temperature results in a significant decrease in strength. Saturation of the separator material in Dimethyl carbonate induces greater compliance upon initial loading in both the machine and transverse directions. Samples saturated in Dimethyl carbonate also showed an increase in toughness over dry samples when loaded in the machine direction. In predicting the mechanical response of the separator the Hybrid Model has shown to provide an adequate prediction if used to describe tensile loading in only one direction. For a more accurate representation of the mechanical properties of the separator in both the machine direction and transverse direction simultaneously the Anisotropic Bergstrom Boyce constitutive model is preferred.

REFERENCES

Arora, P., & Zhang, Z. J. (2004). Battery separators. *Chemical reviews*, *104*(10), 4419–62. Retrieved from http://www.ncbi.nlm.nih.gov/pubmed/15669158

Arruda, E. M., & Boyce, M. C. (1993). A three-dimensional constitutive model for the large stretch behavior of rubber elastic materials. *Journal of Mechanics and Physics of Solids1*, *46*, 389–412.

Bergstrom, J. S. (1999). *Large Strain Time-Dependent Behavior of Elastomeric Materials*. MIT.

Bergström, J. S., Kurtz, S. M., Rimnac, C. M., & Edidin, a a. (2002). Constitutive modeling of ultra-high molecular weight polyethylene under large-deformation and cyclic loading conditions. *Biomaterials*, *23*(11), 2329–43. Retrieved from http://www.ncbi.nlm.nih.gov/pubmed/12013180

Bowden, A. E., Oneida, E., & Bergstr, J. (n.d.). Computer Modeling and Simulation of UHMWPE, 519–532.

Callister, W. D., & Rethwisch, D. G. (2010). *Materials Science and Engineering: An Introduction, 8th Edition* (8th ed.). United States of America: John Wiley & Sons, Inc.

Celgard. (2012). Trilayer Polypropylene/Polyethylene (PP/PE/PP). Retrieved from http://www.celgard.com/Trilayer-PP.aspx

Chaboche, J. L. (2008). A review of some plasticity and viscoplasticity constitutive theories. *International Journal of Plasticity*, *24*(10), 1642–1693. doi:10.1016/j.ijplas.2008.03.009

Dimethyl Carbonate MSDS. (2011). Retrieved from http://www.dimethylcarbonate.com/dimethyl_carbonate_msds.html

Drozdov, a. D., & deC. Christiansen, J. (2007). Viscoelasticity and viscoplasticity of semicrystalline polymers: Structure-property relations for high-density polyethylene. *Computational Materials Science*, *39*(4), 729–751. doi:10.1016/j.commatsci.2006.09.001

Gaines, L., & Cuenca, R. (2000). Costs of Lithium-Ion Batteries for Vehicles. (L. Gaines & R. Cuenca, Eds.)*Energy*, *48*(3), 73. doi:10.1002/art.10781

Huang, X. (2010). Separator technologies for lithium-ion batteries. *Journal of Solid State Electrochemistry*, *15*(4), 649–662. doi:10.1007/s10008-010-1264-9

Love, C. T. (2011). Thermomechanical analysis and durability of commercial micro-porous polymer Li-ion battery separators. *Journal*

of Power Sources, *196*(5), 2905–2912.
doi:10.1016/j.jpowsour.2010.10.083

Mikolajczak, C., Kahn, M., White, K., & Long, R. (2012). *Lithium-Ion Batteries Hazard and Use Assessment* (p. 115). Springer. Retrieved from
http://books.google.com/books?hl=en&lr=&id=sRcdxgTXn4UC&oi=fnd&pg=P R6&dq=Lithium-
Ion+Batteries+Hazard+and+Use+Assessment&ots=CkEw3Jpl17&sig=nAfhEg9J fR3Zcf0cqDoFKRBRHMU

Nikolov, S., & Doghri, I. (2000). A micro / macro constitutive model for the small-deformation behavior of polyethylene, *41*, 1883–1891.

PolyUMod; A Library of Advanced User Materials. (n.d.).

RSA III Rheometrics System Analyzer. (2005). New Castle, DE: TA Instruments-Waters LLC.

Sheidaei, A., Xiao, X., Huang, X., & Hitt, J. (2011). Mechanical behavior of a battery separator in electrolyte solutions. *Journal of Power Sources*, *196*(20), 8728–8734.
doi:10.1016/j.jpowsour.2011.06.026

APPENDIX A (saturation chamber design**)**
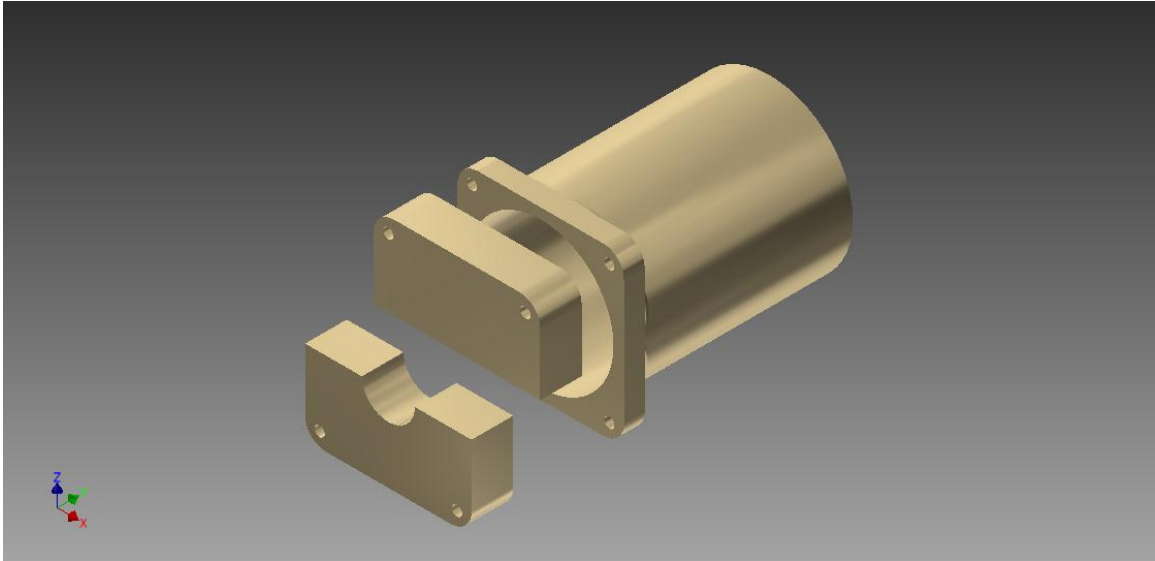
FIGURE 30 IMMERSION FIXTURE DESIGNED TO CLAMP AROUND EXISTING TENSILE TESTER.
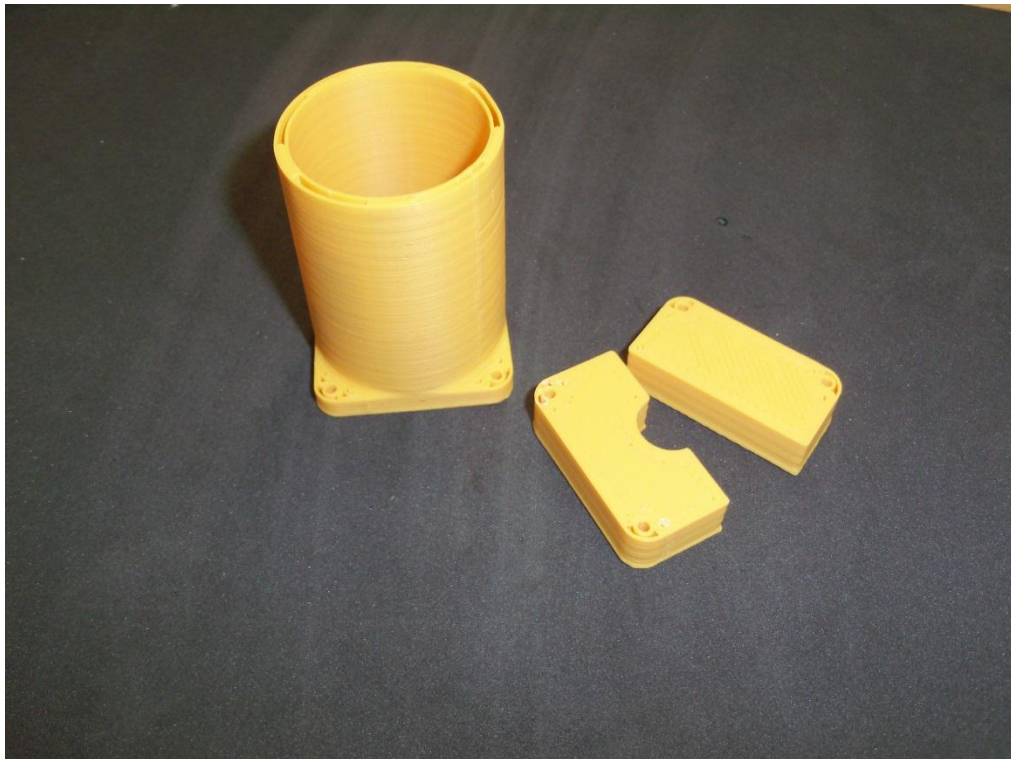
FIGURE 31 3D PRINT OF ORIGINAL FIXTURE DESIGN
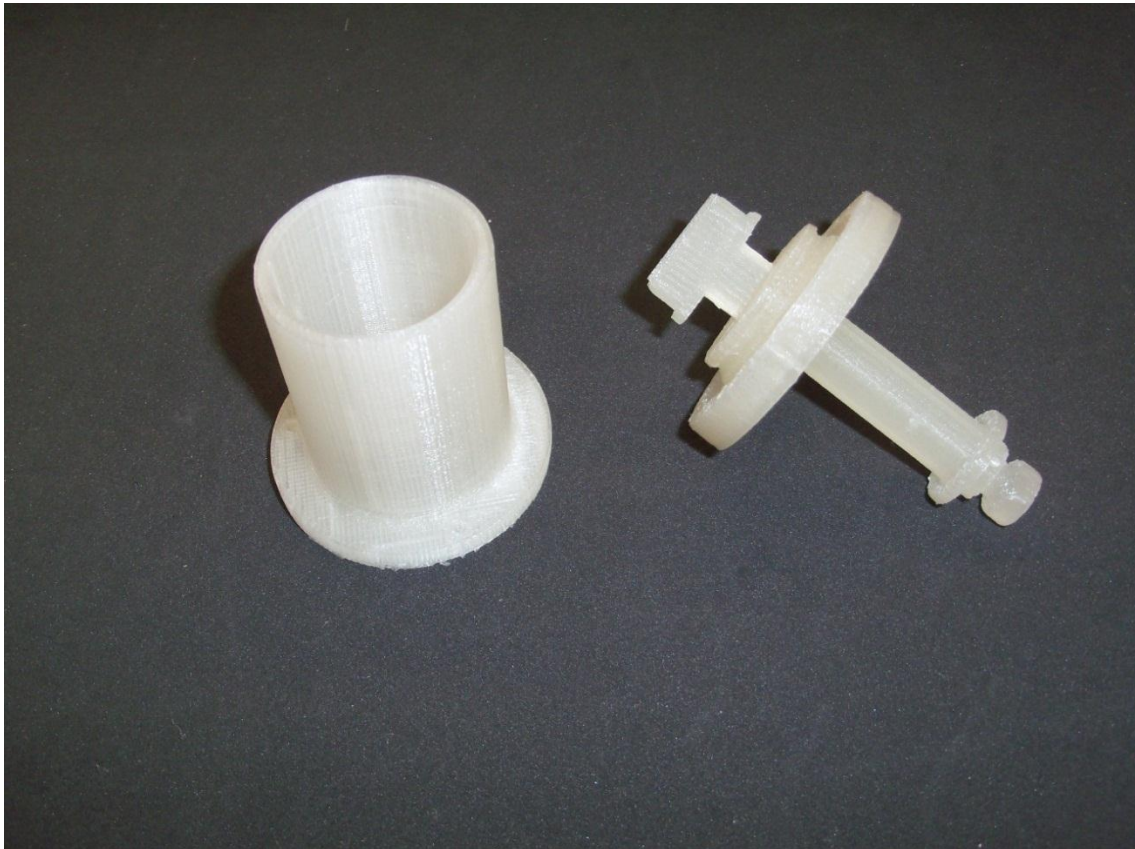
FIGURE 32 FIRST PROOF OF CONCEPT. SMALL CLEARANCES BETWEEN FIXTURE AND TEMPERATURE CHAMBER REQUIRED A REDESIGN.
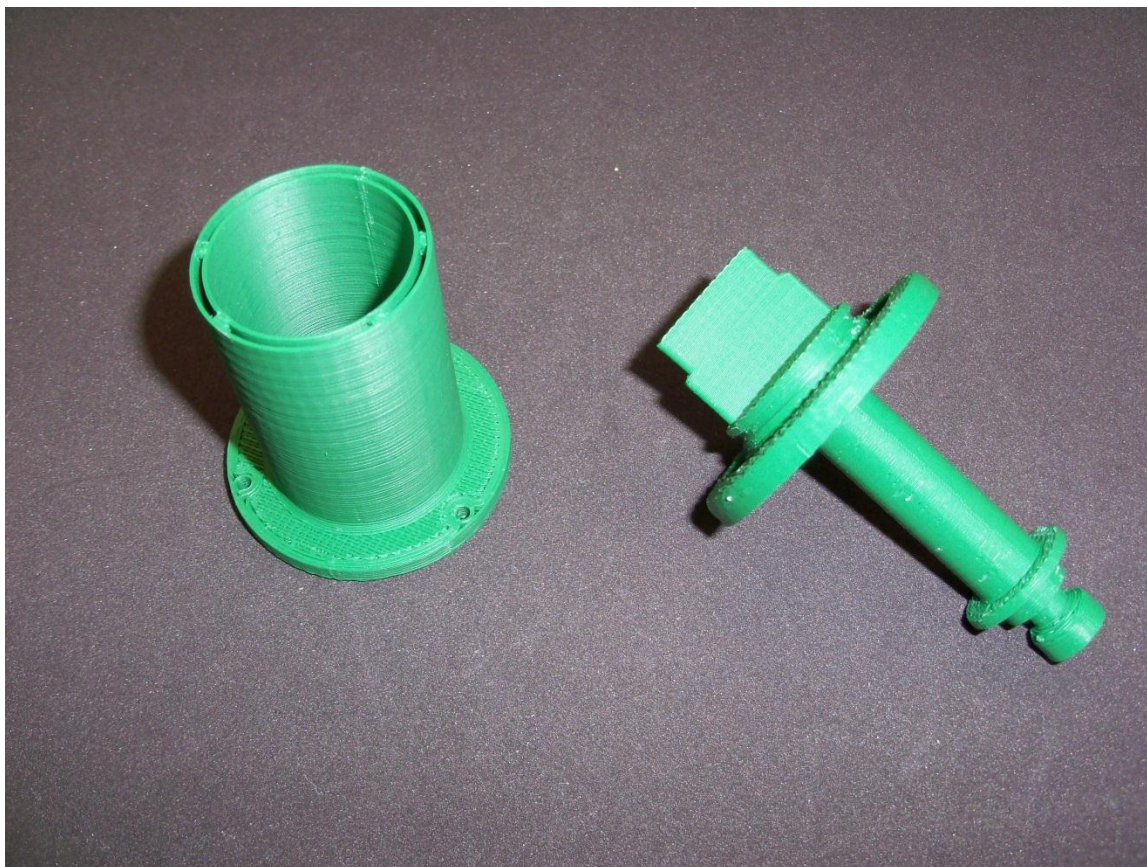
FIGURE 33 TENSILE TESTING FIXTURE DESIGNED WITH SMALLER SATURATION CHAMBER TO REDUCE THE AMOUNT OF SOLVENT NEEDED. ALL BUT THE CLAMPING FACE COULD BE MILLED ON A LATHE TO REDUCE MACHINING TIME.
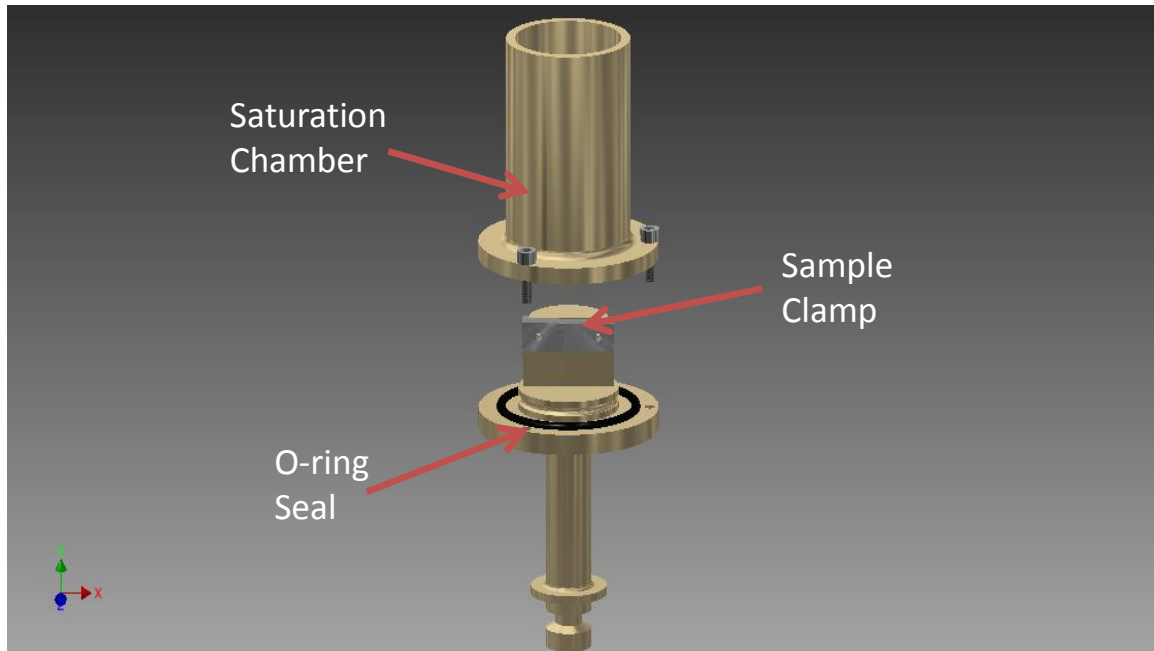
FIGURE 34   FINAL DESIGN.

TWO SEPARATE GROOVES FOR RUBBER O-RING GASKETS WERE MILLED INTO THE TESTING FIXTURE TO CREATE A DOUBLE SEAL.

FIGURE 35 FABRICATED TENSILE TESTER WITH SATURATION CHAMBER

2   1

B   B

.998

.871

.28

.059 .059

.394

R.039

.197

1.535

.049

.157

.079

.130

.175 .498

.833

A   A

DRAWN			
Michael Martinsen	9/21/2012		
CHECKED		TITLE	
QA			
MFG			
APPROVED			

SIZE		DWG NO	REV
A		Tensile Tester	
SCALE			SHEET 2 OF 5

2   1
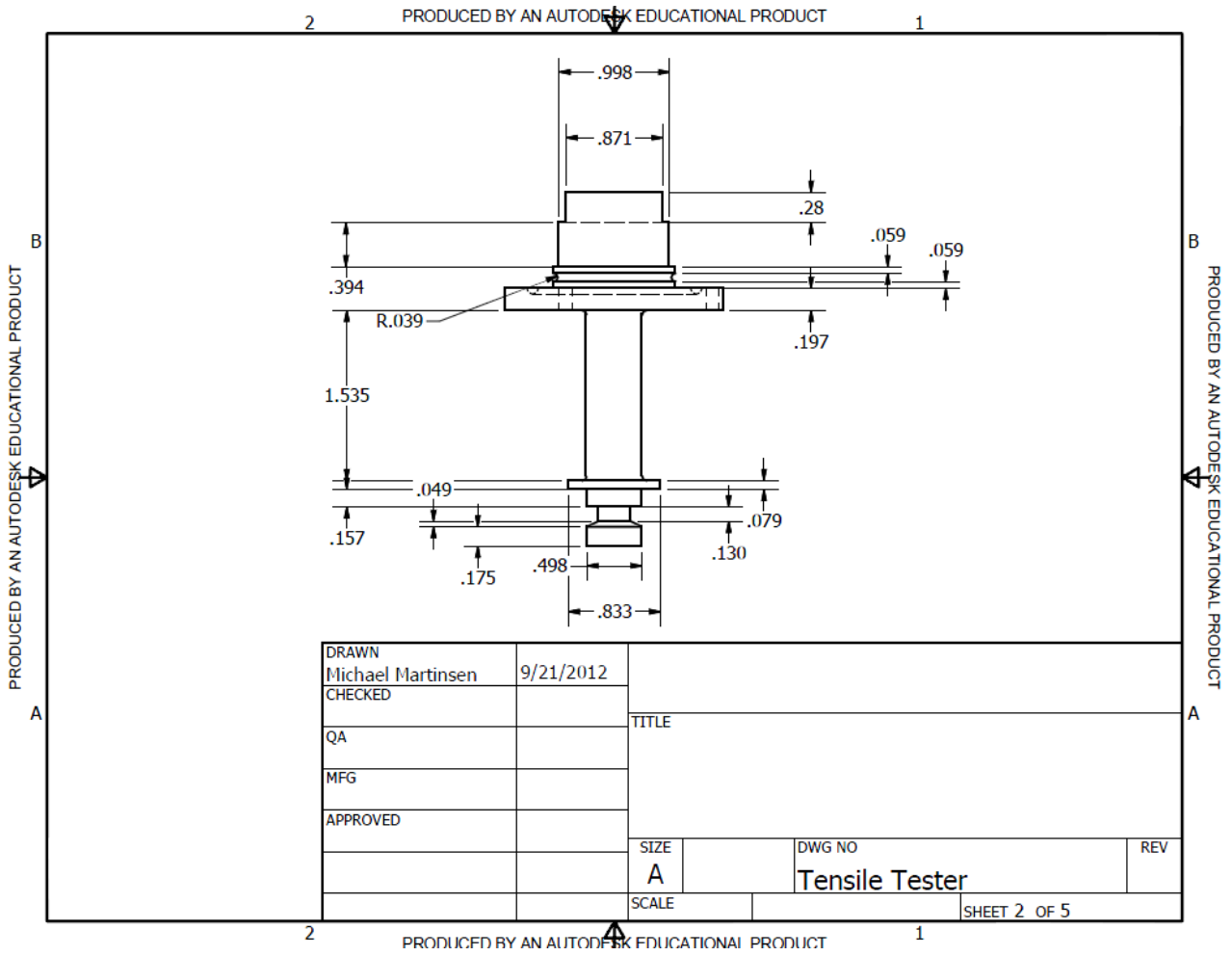
FIGURE 36 ENGINEERING DRAWING TENSILE TESTER (FRONT VIEW)

2 1

1.10
.499
.435

R.049

R.04

B B

A A

DRAWN Michael Martinsen	9/21/2012	
CHECKED		TITLE
QA		
MFG		
APPROVED		
		SIZE A / DWG NO Tensile Tester / REV
		SCALE / SHEET 3 OF 5

2 1
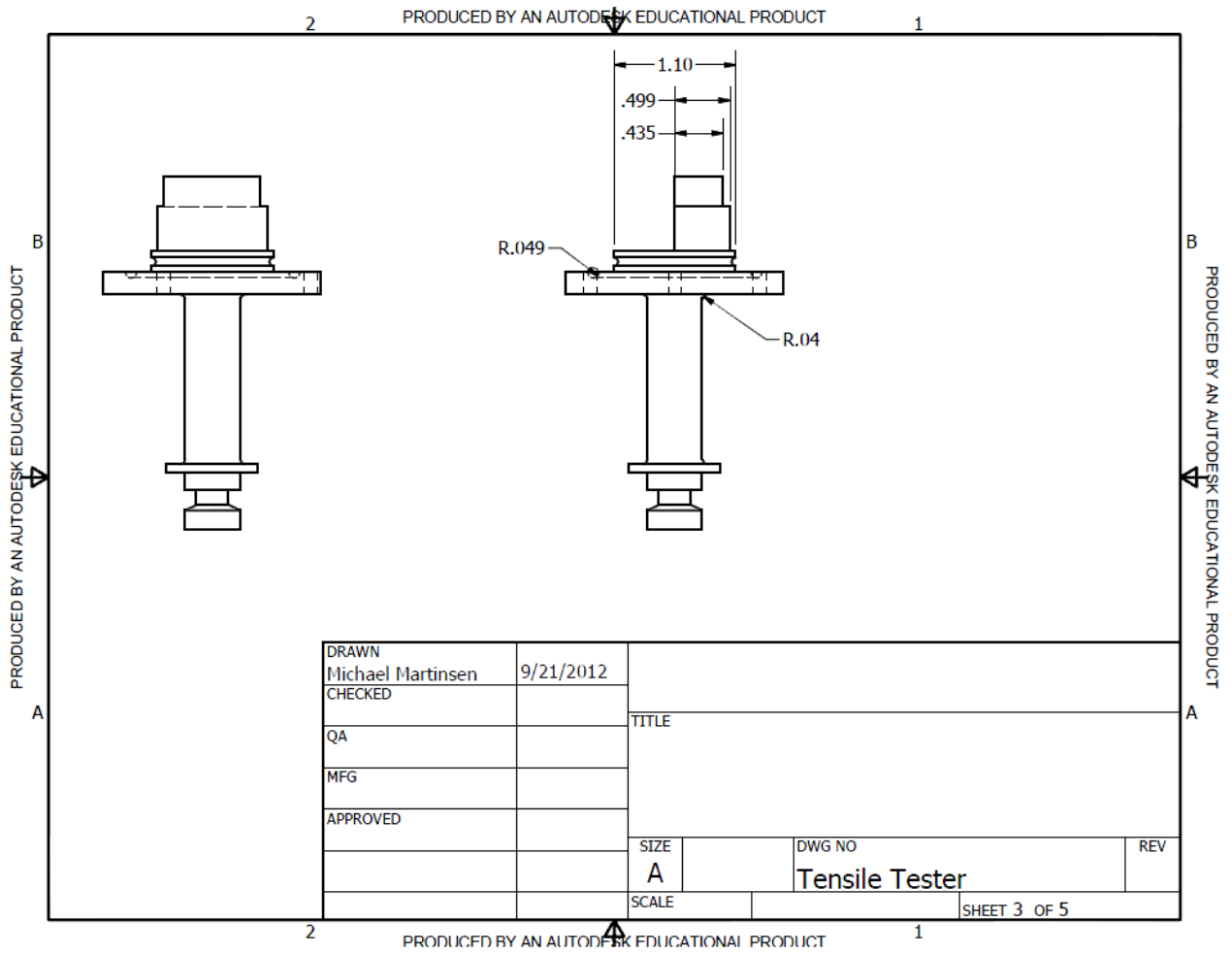
FIGURE 37 ENGINEERING DRAWING TENSILE TESTER (SIDE VIEW)

R.499
Ø1.969
Ø.291
R.435
Ø1.575
Ø.502
Ø1.378
Ø1.024
Ø.833
Ø1.102

DRAWN						
Michael Martinsen	9/21/2012					
CHECKED						
QA		TITLE				
MFG						
APPROVED						
		SIZE	DWG NO			REV
		A	Tensile Tester			
		SCALE			SHEET 4 OF 5	
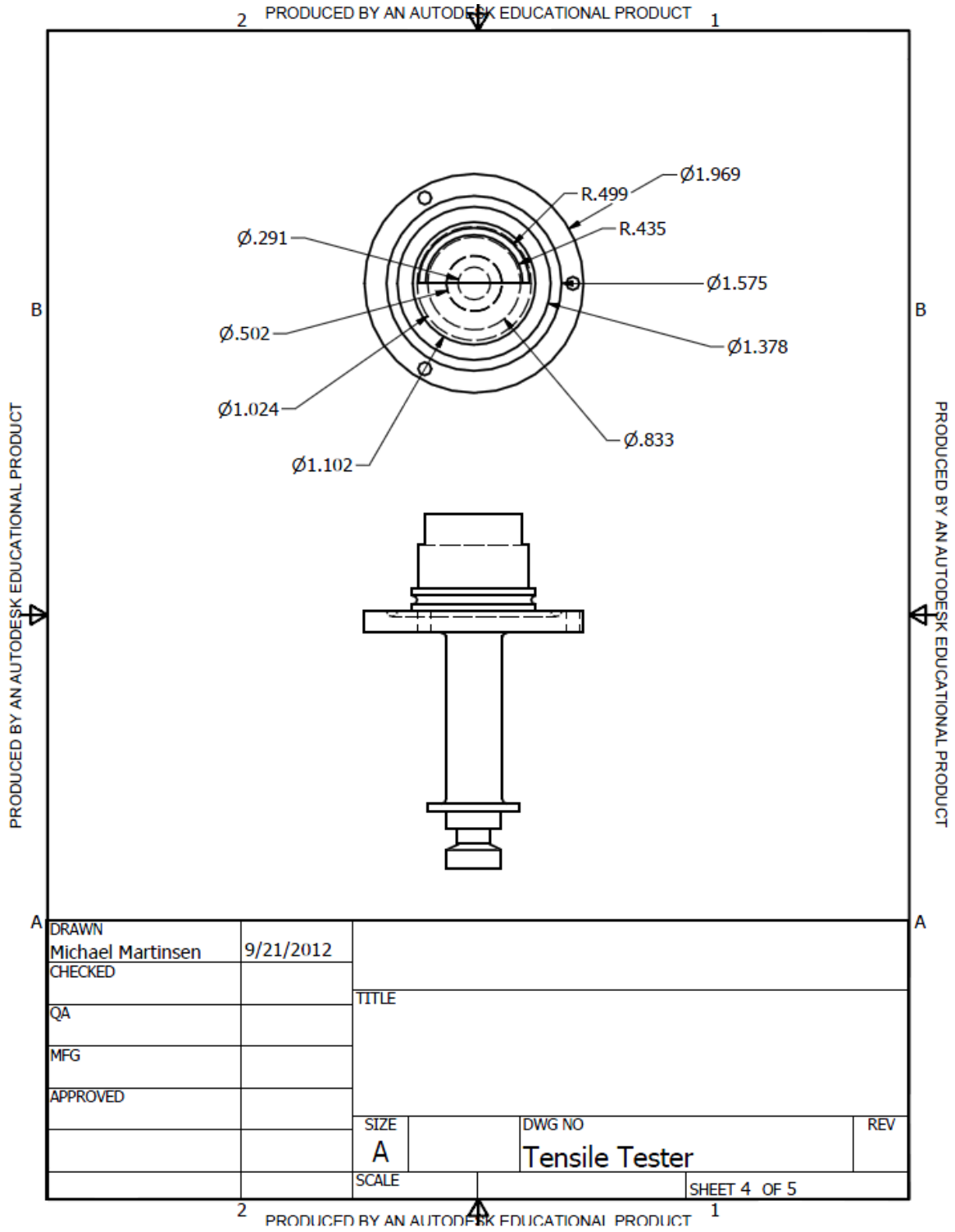
FIGURE 38   ENGINEERING DRAWING TENSILE TESTER (TOP VIEW)

Ø1.969

Ø1.161

Ø1.358

1.969

R.079

.157

DRAWN		
Michael Martinsen	9/21/2012	
CHECKED		
QA		TITLE
MFG		Sleve
APPROVED		

SIZE	DWG NO	REV
A	Tensile Tester	
SCALE	SHEET 5 OF 5	
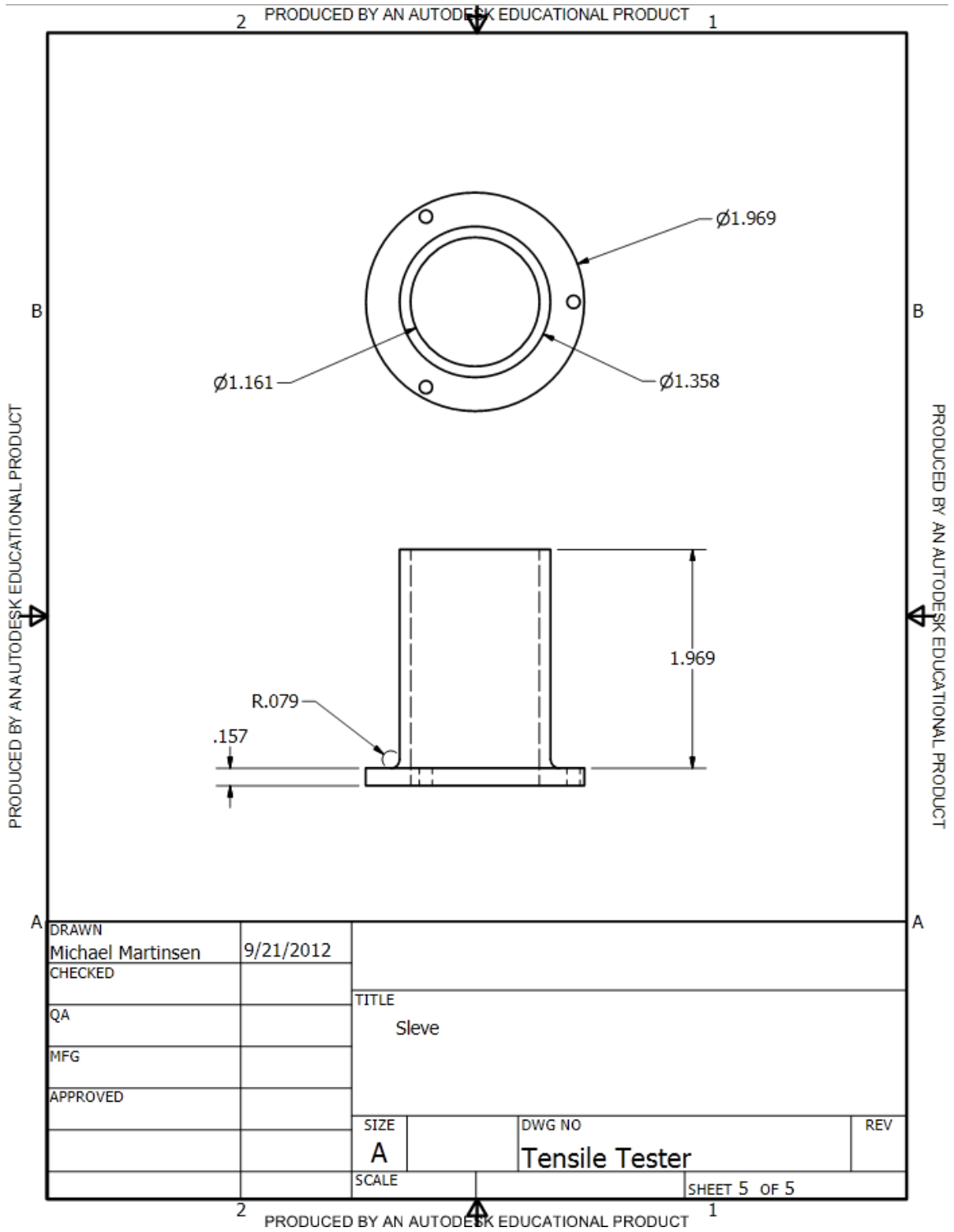
FIGURE 39 ENGINEERING DRAWING SATURATION CHAMBER

APPENDIX B (comparison of wet and dry samples**)**

FIGURE 40 COMPARRISON OF SATURATED AND DRY SAMPLES AT 28.5°C AND 0.001/S STRAIN RATE (MACHINE DIRECTION)

FIGURE 41 COMPARRISON OF SATURATED AND DRY SAMPLES AT 28.5°C AND 0.01/S STRAIN RATE (MACHINE DIRECTION)

FIGURE 42   COMPARRISON OF SATURATED AND DRY SAMPLES AT 28.5°C AND 0.1/S STRAIN RATE (MACHINE DIRECTION)

FIGURE 43 COMPARRISON OF SATURATED AND DRY SAMPLES AT 28.5°C AND 0.001/S STRAIN RATE (TRANSVERSE DIRECTION)

FIGURE 44 COMPARRISON OF SATURATED AND DRY SAMPLES AT 28.5°C AND 0.01/S STRAIN RATE (TRANSVERSE DIRECTION)

FIGURE 45 COMPARRISON OF SATURATED AND DRY SAMPLES AT 28.5°C AND 0.1/S STRAIN RATE (TRANSVERSE DIRECTION)
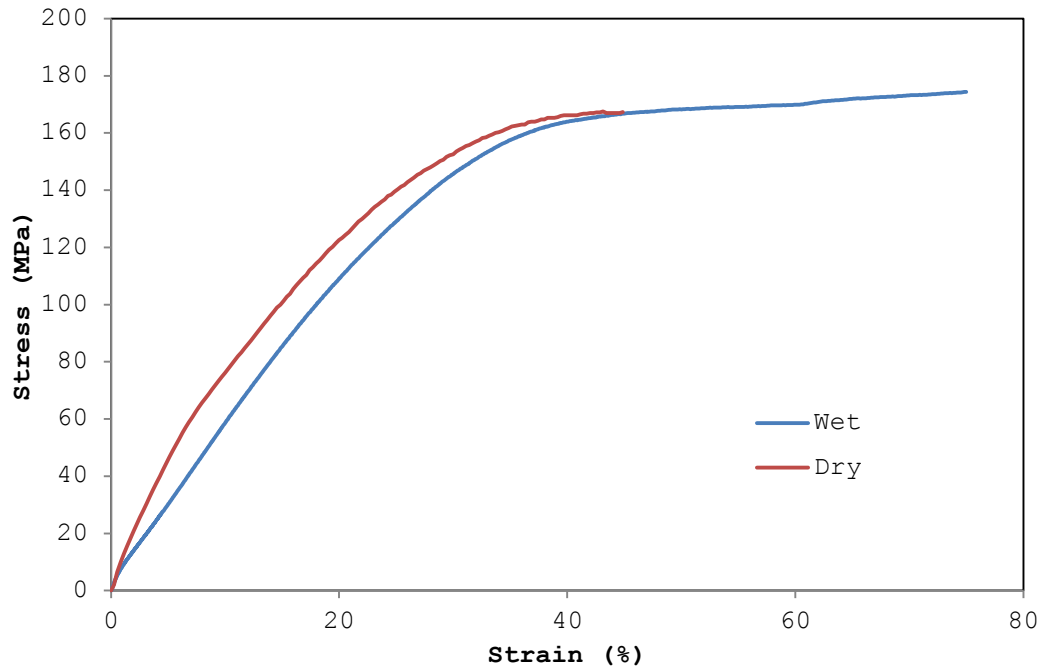
FIGURE 46   COMPARRISON OF SATURATED AND DRY SAMPLES AT 28.5°C AND 0.01/S STRAIN RATE (MACHINE DIRECTION)
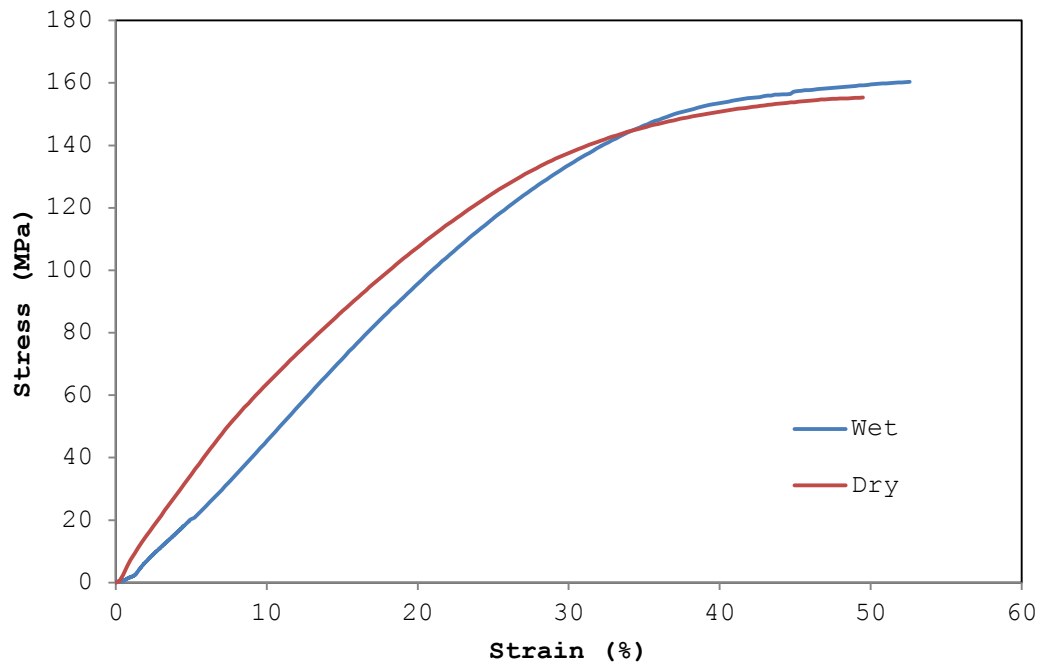
FIGURE 47 COMPARRISON OF SATURATED AND DRY SAMPLES AT 55°C AND 0.01/S STRAIN RATE (MACHINE DIRECTION)
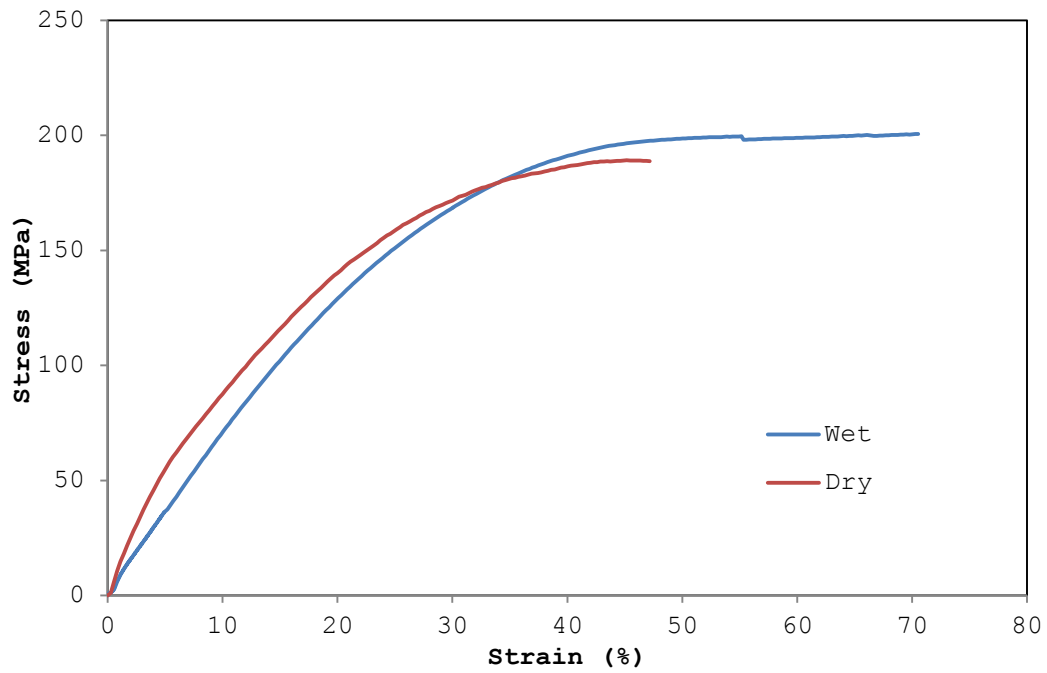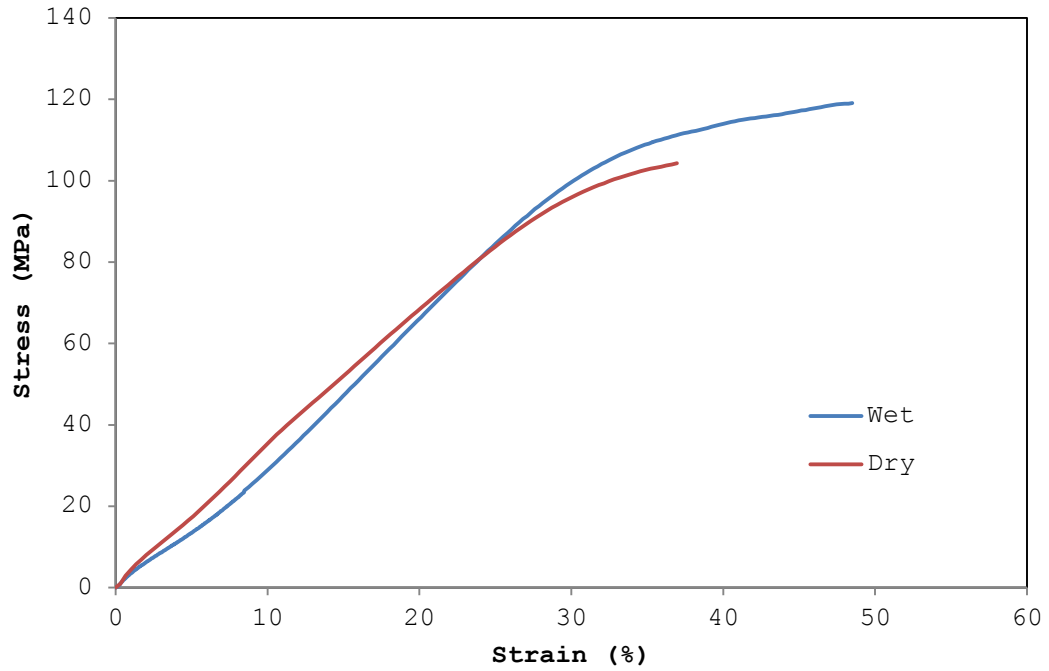
FIGURE 48 COMPARRISON OF SATURATED AND DRY SAMPLES AT 80°C AND 0.01/S STRAIN RATE (MACHINE DIRECTION)
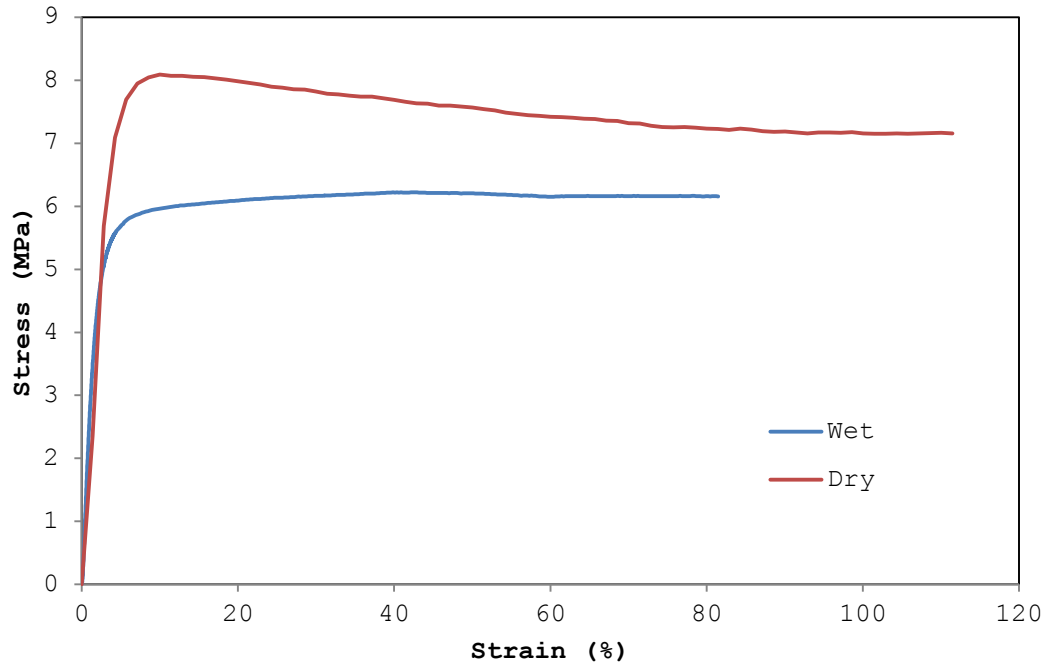
FIGURE 49 COMPARRISON OF SATURATED AND DRY SAMPLES AT 28.5°C AND 0.01/S STRAIN RATE (TRANSVERSE DIRECTION)
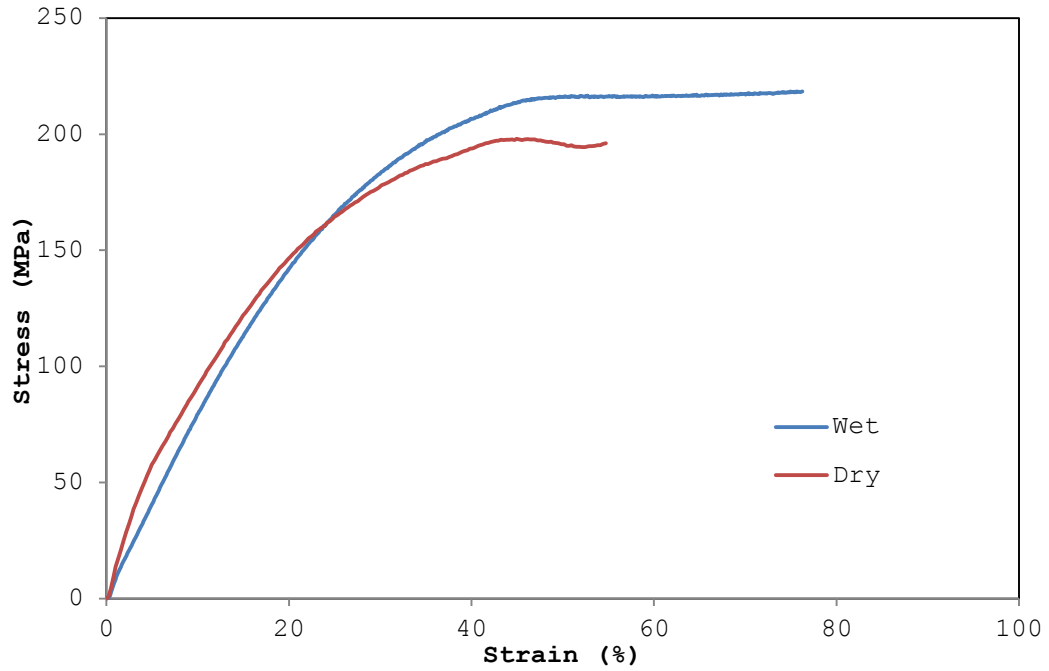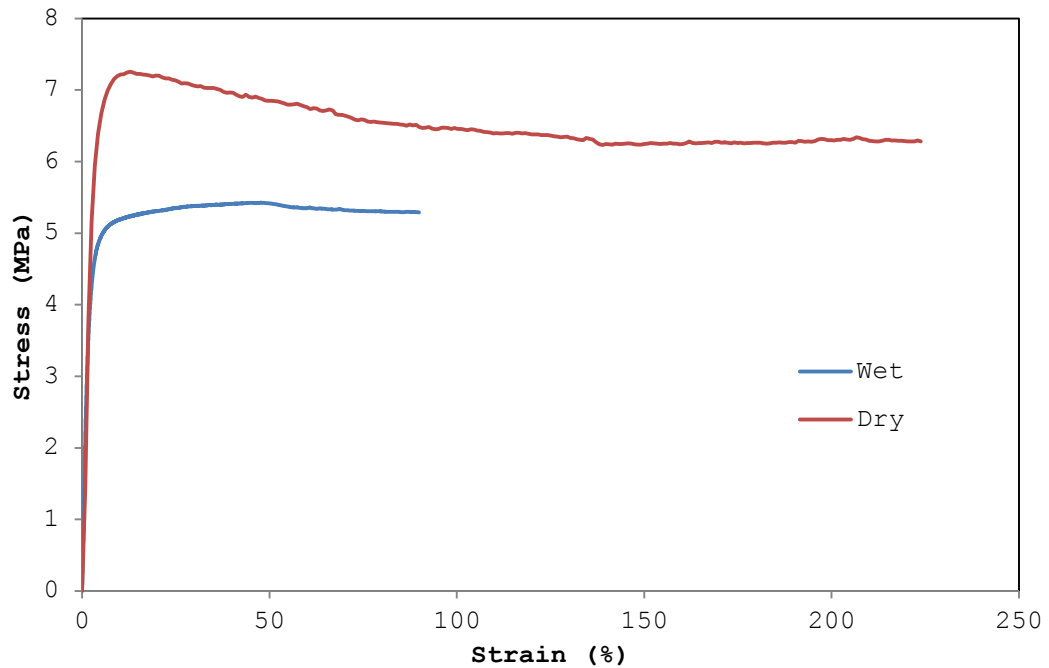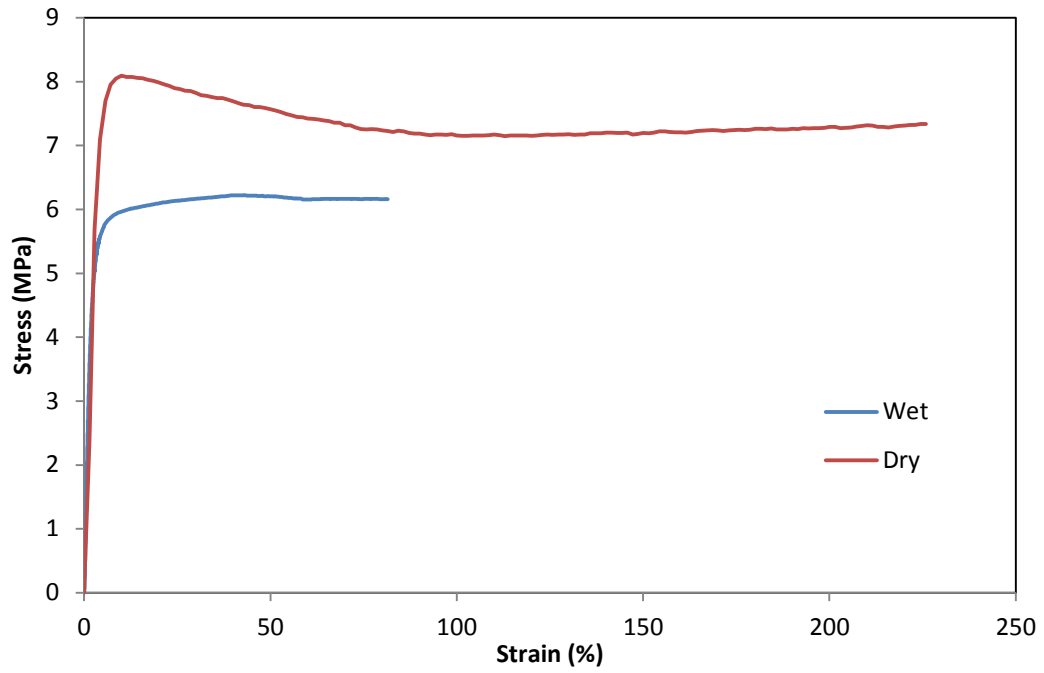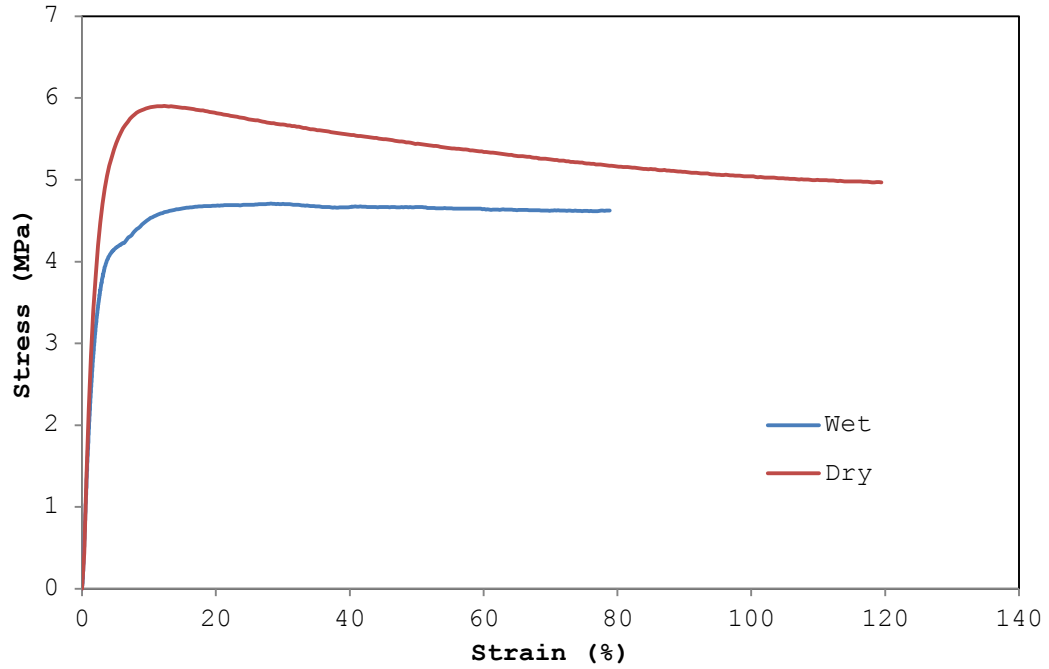
FIGURE 50 COMPARRISON OF SATURATED AND DRY SAMPLES AT 55°C AND 0.01/S
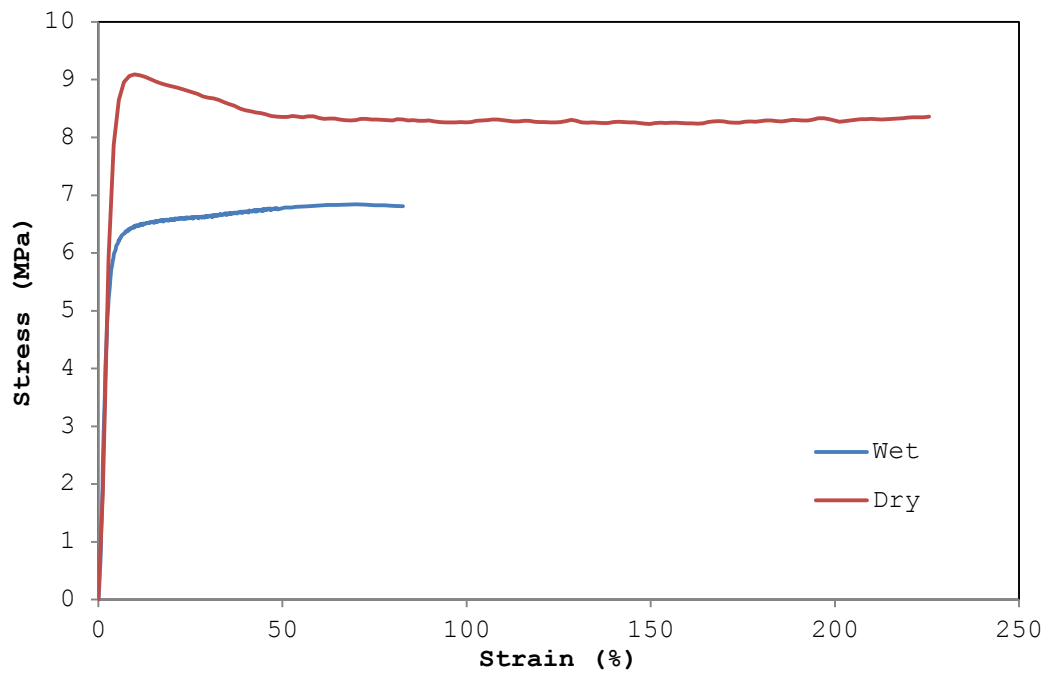STRAIN RATE (TRANSVERSE DIRECTION)
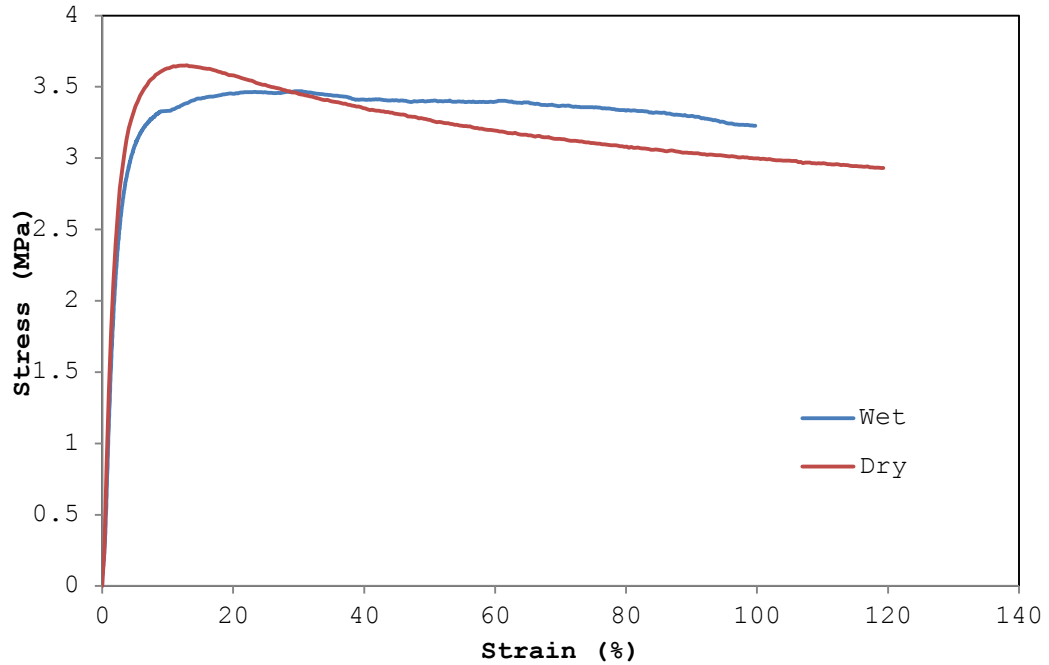
FIGURE 51 COMPARRISON OF SATURATED AND DRY SAMPLES AT 80°C AND 0.01/S
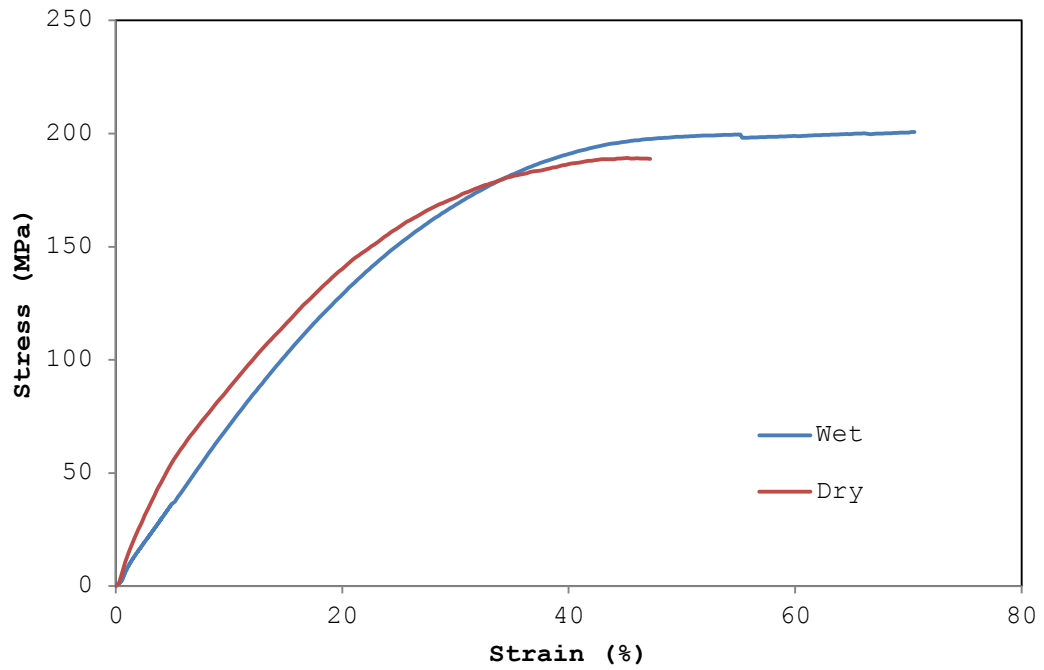STRAIN RATE (TRANSVERSE DIRECTION)

APPENDIX C

ANSYS Code for Hybrid Model (Machine Direction)

```
! PolyUMod defined material model -- start

!   Units:    [length]=millimeter,    [force]=Newton,    [time]=seconds,
[temperature]=Kelvin

! Material Model: Hybrid-Model

! Calibration file name: Machine Direction(1).txt.mcal


! (delete any current user-material with id=matid)

TBDELE, ALL, matid


! (define  material  matid  to  be  a  user-material  with  the  specified
number of material parameters)

! order: TB, Lab, MAT, NTEMP, NPTS

TB, USER, matid, 1, 30


! (the provided material parameters are for the following temperature)

TBTEMP, 0


! (define the actual material parameters)

TBDATA, 1, 7            ! MM

TBDATA, 2, 0            ! ODE

TBDATA, 3, 0            ! JAC

TBDATA, 4, 0            ! ERRM

TBDATA, 5, 0            ! TWOD_S

TBDATA, 6, 1            ! VERB

TBDATA, 7, 0            ! VTIME
```

```
TBDATA, 8, 0              ! VELEM

TBDATA, 9, 0              ! VINT

TBDATA, 10, 0             ! ORIENT

TBDATA, 11, 30            ! NPROP

TBDATA, 12, 23            ! NHIST

TBDATA, 13, 1             ! GMU

TBDATA, 14, 500           ! GKAPPA

TBDATA, 15, 0             ! FAILT

TBDATA, 16, 0             ! FAILV

TBDATA, 17, 2560.58           ! Ee

TBDATA, 18, 0.498472          ! nuE

TBDATA, 19, 170.026           ! muA

TBDATA, 20, 5.13226           ! lamdaLA

TBDATA, 21, 0.00829032391294       ! q

TBDATA, 22, 96131.1           ! kappaA

TBDATA, 23, 30.9674920631         ! sBi

TBDATA, 24, 1.46574           ! sBf

TBDATA, 25, 23287.11525       ! alphaB

TBDATA, 26, 292.613           ! tauBaseB

TBDATA, 27, 3.49261           ! mB

TBDATA, 28, 906.687           ! pHat

TBDATA, 29, 133.093           ! tauBaseP

TBDATA, 30, 2.29385           ! mP


! (delete old state variables)

!TBDELE, STATE, matid


! (define new state variables)

! order: TB, Lab, MAT, NTEMP, NPTS
```

```
TB, STATE, matid, 1, 23

TBTEMP, 0

TBDATA, 1, 0.0

TBDATA, 2, 0.0

TBDATA, 3, 0.0

TBDATA, 4, 0.0

TBDATA, 5, 0.0

TBDATA, 6, 0.0

TBDATA, 7, 0.0

TBDATA, 8, 0.0

TBDATA, 9, 0.0

TBDATA, 10, 0.0

TBDATA, 11, 0.0

TBDATA, 12, 0.0

TBDATA, 13, 0.0

TBDATA, 14, 0.0

TBDATA, 15, 0.0

TBDATA, 16, 0.0

TBDATA, 17, 0.0

TBDATA, 18, 0.0

TBDATA, 19, 0.0

TBDATA, 20, 0.0

TBDATA, 21, 0.0

TBDATA, 22, 0.0

TBDATA, 23, 0.0


MP, DENS, matid, 1e-09


! PolyUMod defined material model – end
```

ANSYS Code for Hybrid Model (Transverse Direction)

```
! PolyUMod defined material model -- start

!   Units:   [length]=millimeter,   [force]=Newton,   [time]=seconds,
[temperature]=Kelvin

! Material Model: Hybrid-Model

! Calibration file name: Hybrid Model (TD).mcal


! (delete any current user-material with id=matid)

TBDELE, ALL, matid


! (define material matid to be a user-material with the specified
number of material parameters)

! order: TB, Lab, MAT, NTEMP, NPTS

TB, USER, matid, 1, 30


! (the provided material parameters are for the following temperature)

TBTEMP, 0


! (define the actual material parameters)

TBDATA, 1, 7            ! MM

TBDATA, 2, 0            ! ODE

TBDATA, 3, 0            ! JAC

TBDATA, 4, 0            ! ERRM

TBDATA, 5, 0            ! TWOD_S

TBDATA, 6, 1            ! VERB

TBDATA, 7, 0            ! VTIME

TBDATA, 8, 0            ! VELEM
```

```
TBDATA, 9, 0               ! VINT

TBDATA, 10, 0              ! ORIENT

TBDATA, 11, 30             ! NPROP

TBDATA, 12, 23             ! NHIST

TBDATA, 13, 1              ! GMU

TBDATA, 14, 500            ! GKAPPA

TBDATA, 15, 0              ! FAILT

TBDATA, 16, 0              ! FAILV

TBDATA, 17, 4864.38019542            ! Ee

TBDATA, 18, 0.46           ! nuE

TBDATA, 19, 0.930926432914           ! muA

TBDATA, 20, 3.77890186316            ! lamdaLA

TBDATA, 21, 0.01           ! q

TBDATA, 22, 1312.61            ! kappaA

TBDATA, 23, 39.9911293228            ! sBi

TBDATA, 24, 46.8965349382            ! sBf

TBDATA, 25, 64.8598657113            ! alphaB

TBDATA, 26, 8.53974618952            ! tauBaseB

TBDATA, 27, 10.8705086725            ! mB

TBDATA, 28, 52.5046            ! pHat

TBDATA, 29, 2.96472813975            ! tauBaseP

TBDATA, 30, 4.26200015181            ! mP


! (delete old state variables)

!TBDELE, STATE, matid


! (define new state variables)

! order: TB, Lab, MAT, NTEMP, NPTS

TB, STATE, matid, 1, 23
```

```
TBTEMP, 0

TBDATA, 1, 0.0

TBDATA, 2, 0.0

TBDATA, 3, 0.0

TBDATA, 4, 0.0

TBDATA, 5, 0.0

TBDATA, 6, 0.0

TBDATA, 7, 0.0

TBDATA, 8, 0.0

TBDATA, 9, 0.0

TBDATA, 10, 0.0

TBDATA, 11, 0.0

TBDATA, 12, 0.0

TBDATA, 13, 0.0

TBDATA, 14, 0.0

TBDATA, 15, 0.0

TBDATA, 16, 0.0

TBDATA, 17, 0.0

TBDATA, 18, 0.0

TBDATA, 19, 0.0

TBDATA, 20, 0.0

TBDATA, 21, 0.0

TBDATA, 22, 0.0

TBDATA, 23, 0.0




MP, DENS, matid, 1e-09



! PolyUMod defined material model -- end
```

ANSYS Code for Anisotropic Bergstrom-Boyce Model

```
! PolyUMod defined material model -- start

!   Units:    [length]=millimeter,    [force]=Newton,    [time]=seconds,
[temperature]=Kelvin

! Material Model: Parallel-Network-Model

! Calibration file name: simulation3.mcal


! (delete any current user-material with id=matid)

TBDELE, ALL, matid


! (define material matid to be a user-material with the specified
number of material parameters)

! order: TB, Lab, MAT, NTEMP, NPTS

TB, USER, matid, 1, 39


! (the provided material parameters are for the following temperature)

TBTEMP, 0


! (define the actual material parameters)

TBDATA, 1, 14           ! MM

TBDATA, 2, 0            ! ODE

TBDATA, 3, 0            ! JAC

TBDATA, 4, 0            ! ERRM

TBDATA, 5, 0            ! TWOD_S

TBDATA, 6, 1            ! VERB

TBDATA, 7, 0            ! VTIME

TBDATA, 8, 0            ! VELEM

TBDATA, 9, 0            ! VINT

TBDATA, 10, 0          ! ORIENT
```

```
TBDATA, 11, 39          ! NPROP

TBDATA, 12, 13          ! NHIST

TBDATA, 13, 1           ! GMU

TBDATA, 14, 500         ! GKAPPA

TBDATA, 15, 0           ! FAILT

TBDATA, 16, 0           ! FAILV

TBDATA, 17, 2           ! EType

TBDATA, 18, 485.985047568          ! mu

TBDATA, 19, 710.553717573          ! kappa

TBDATA, 20, 505         ! FType

TBDATA, 21, 4.10767397596e-08      ! xi

TBDATA, 22, -0.524078317163        ! C

TBDATA, 23, 72.2956347414          ! tauHat

TBDATA, 24, 5           ! m

TBDATA, 25, 30.5066636619          ! F

TBDATA, 26, 0.0186767909293        ! G

TBDATA, 27, 0.0186767909293        ! H

TBDATA, 28, 3.13808599255          ! L

TBDATA, 29, 2.29600316491          ! M

TBDATA, 30, 3.25538619649          ! N

TBDATA, 31, 805         ! FYE_Type

TBDATA, 32, 2.03402312372          ! ff

TBDATA, 33, 0.0913973240726        ! epsHat

TBDATA, 34, 43.2368488904          ! F

TBDATA, 35, 0.896377653875         ! G

TBDATA, 36, 9.98199551845          ! H

TBDATA, 37, 1           ! L

TBDATA, 38, 1           ! M

TBDATA, 39, 1           ! N
```

```
! (delete old state variables)

!TBDELE, STATE, matid


! (define new state variables)

! order: TB, Lab, MAT, NTEMP, NPTS

TB, STATE, matid, 1, 13

TBTEMP, 0

TBDATA, 1, 0.0

TBDATA, 2, 0.0

TBDATA, 3, 0.0

TBDATA, 4, 0.0

TBDATA, 5, 0.0

TBDATA, 6, 0.0

TBDATA, 7, 0.0

TBDATA, 8, 0.0

TBDATA, 9, 0.0

TBDATA, 10, 0.0

TBDATA, 11, 0.0

TBDATA, 12, 0.0

TBDATA, 13, 0.0



MP, DENS, matid, 1e-09


! PolyUMod defined material model -- end
```